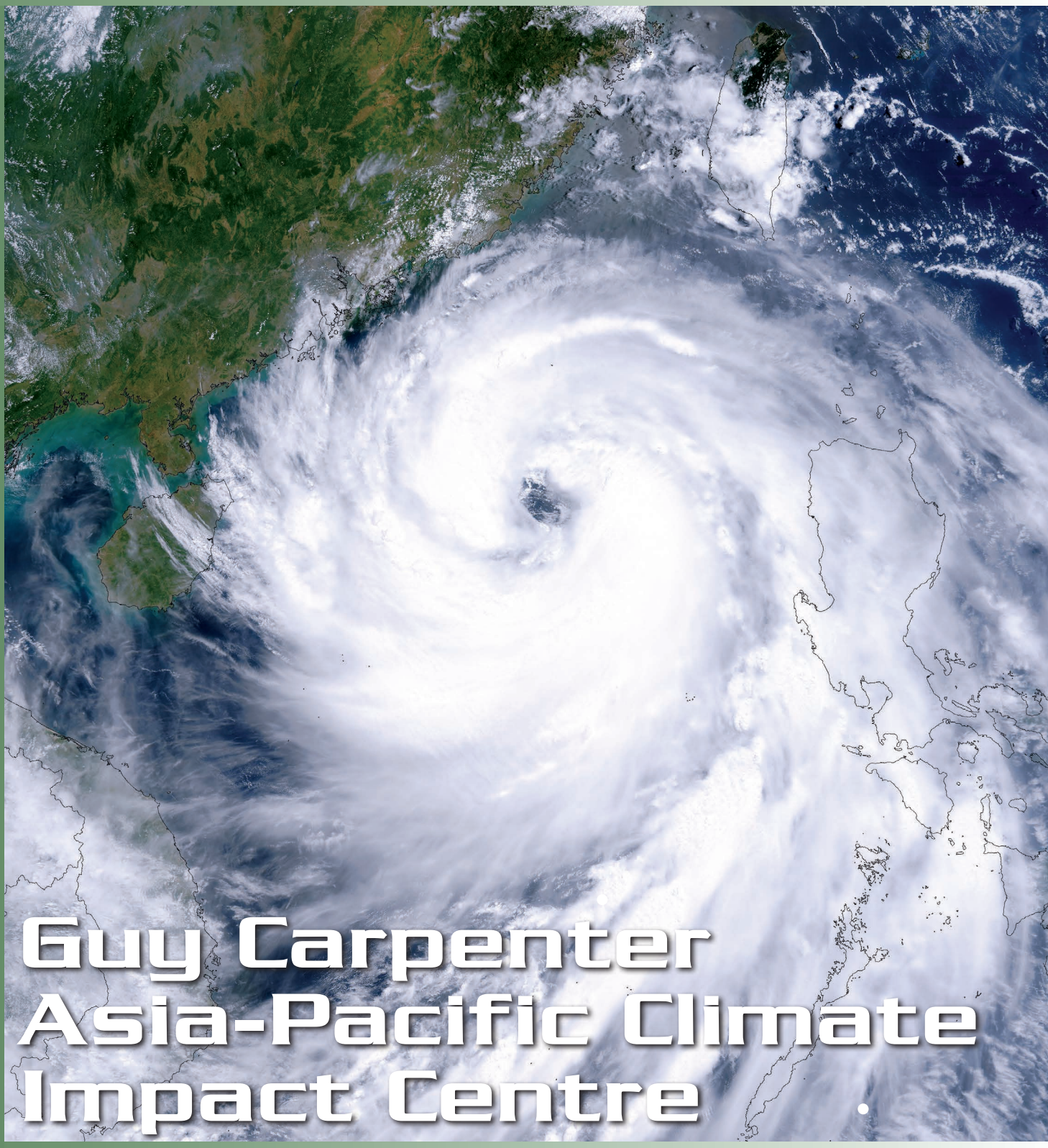

Guy Carpenter Asia-Pacific Climate Impact Centre

Annual Report 2014

GCACIC
Guy Carpenter Asia-Pacific Climate Impact Centre
City University of Hong Kong

香港城市大學
City University of Hong Kong

Published May 2015

Executive Summary

This is the sixth annual report issued by the Guy Carpenter Asia-Pacific Climate Impact Centre and covers the activities of the Centre in 2014. A major focus of our work continues to be on improving our understanding of the physical processes responsible for different types of climate variability in our region, which included winter temperatures, heavy precipitation, regional droughts, and tropical cyclone damage (winds and precipitation). In addition, based on the latest climate projections, we studied possible changes to the start of the growing season as well as atmospheric circulation under various climate change scenarios. We continued to work on the problem of air pollution in the region, both in terms of measurements and modeling of the effects of different pollutants on local and regional climate.

The report is divided into four sections, with a total of 18 projects. Section A is on climate change and projection using model projections from the various climate models. Section B contains studies focusing on climate variability of different phenomena affecting the Asia-Pacific region, including the number of cold days, summertime persistent heavy precipitation and autumn precipitation. Section C examines the variations of tropical cyclone damage along the East Asia coast, and tropical cyclone precipitation in southeast China and Hong Kong. Section D reports on studies related to measurements of various pollutant species and model predictions of air pollution episodes.

As in the past, the main results from each of the projects are briefly described in this report. The papers produced from these projects are available either from the CD attached to the report or from our website.

Contents

I. Introduction

The Guy Carpenter Asia-Pacific Climate Impact Centre was established in June 2008. Since 2009, we have been issuing an annual report that describes our research activities during the year, and this is our sixth annual report that describes the activities of the Centre in 2014. During the year, we continued to work on climate problems related to Hong Kong, the Asia-Pacific region as well as those on a global scale, with a total of 18 projects. For each project, we summarise the main results for the reader to have a quick introduction of the subject. In most cases, the results have been published in one or more journal articles, which are listed at the end of the summary of each project. A copy of each of the publications is included in the CD attached to the report and is also available online at http://www.cityu.edu.hk/gcacic/publications.htm.

We hope that this report will provide the reader of an overall picture of the research activities of the Centre. Suggestions and comments on the projects are most welcome

II. Research Projects

A. Climate Change and Projection

A1. Projections of advance in the start of growing season during the 21st century

(PI: Wen ZHOU)

It is well-known that global warming due to anthropogenic atmospheric greenhouse effects advanced the start of the vegetation growing season (SOS) across the globe during the 20th century. By around 2040--59, the SOS will have advanced by –4.7 days under RCP2.6, –8.4 days under RCP4.5, and –10.1 days under RCP8.5, relative to 1985--2004. By 2080--99, it will have advanced by –4.3 days under RCP2.6, –11.3 days under RCP4.5, and –21.6 days under RCP8.5 (Figure 1). For more details, please refer to Xia et al. (2014).

Projections of further changes in the start of the growing season for the 21st century under certain emissions scenarios (Representative Concentration Pathways, RCPs) are useful for improving our understanding of the effects of global warming on agriculture.

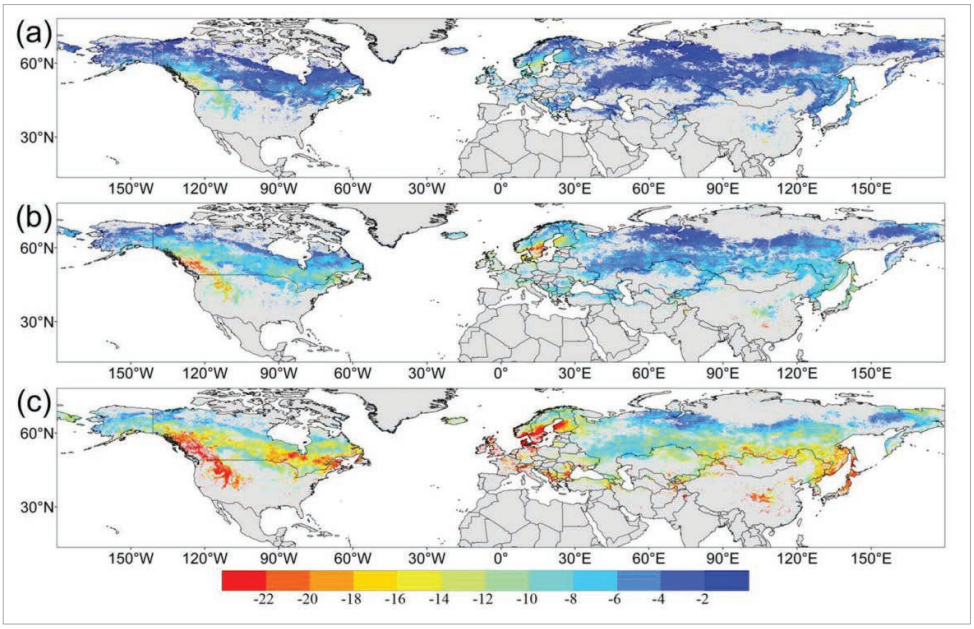

Figure 1. Changes in SOS for (a) RCP2.6, (b) RCP4.5, (c) RCP8.5 for the period 2080-2099 with respect to the results of 1985-2004 under 'historical' scenario, from MME. Units: days

Reference:

Xia J. J., Z. W. Yan, G.S. Jia, H.Q. Zeng, Philip Jones, W. Zhou, A. Z. Zhang, 2014: projections of advanceinthe start of growing season during the 21st century based on CMIP5 simulations. *Adv. Atmos. Sci.*, doi: 10.1007/s00376-014-4125-0.

A2. Implications of Ural Blocking for East Asian Winter Climate in the CMIP5 Models

(PI: Wen ZHOU)

This study consists of two parts (part I and II).

This study investigates the linkage between Ural blocking (UB) and the East Asian winter climate in general circulation modes (GCMs) from the Couple Model Intercomparison Project Phase 5 (CMIP5).

Part I of this work assesses the ability of the 25 CMIP5 GCMs to simulate the Ural Blocking – East Asian winter climate linkage in a historical run (1950/51–2004/05). It was found that the long-term mean bias of Ural blocking frequency (UBI) is caused by the long-term mean circulation bias over the North Atlantic, which is related to the North Atlantic Oscillation (NAO) (Figure 2).

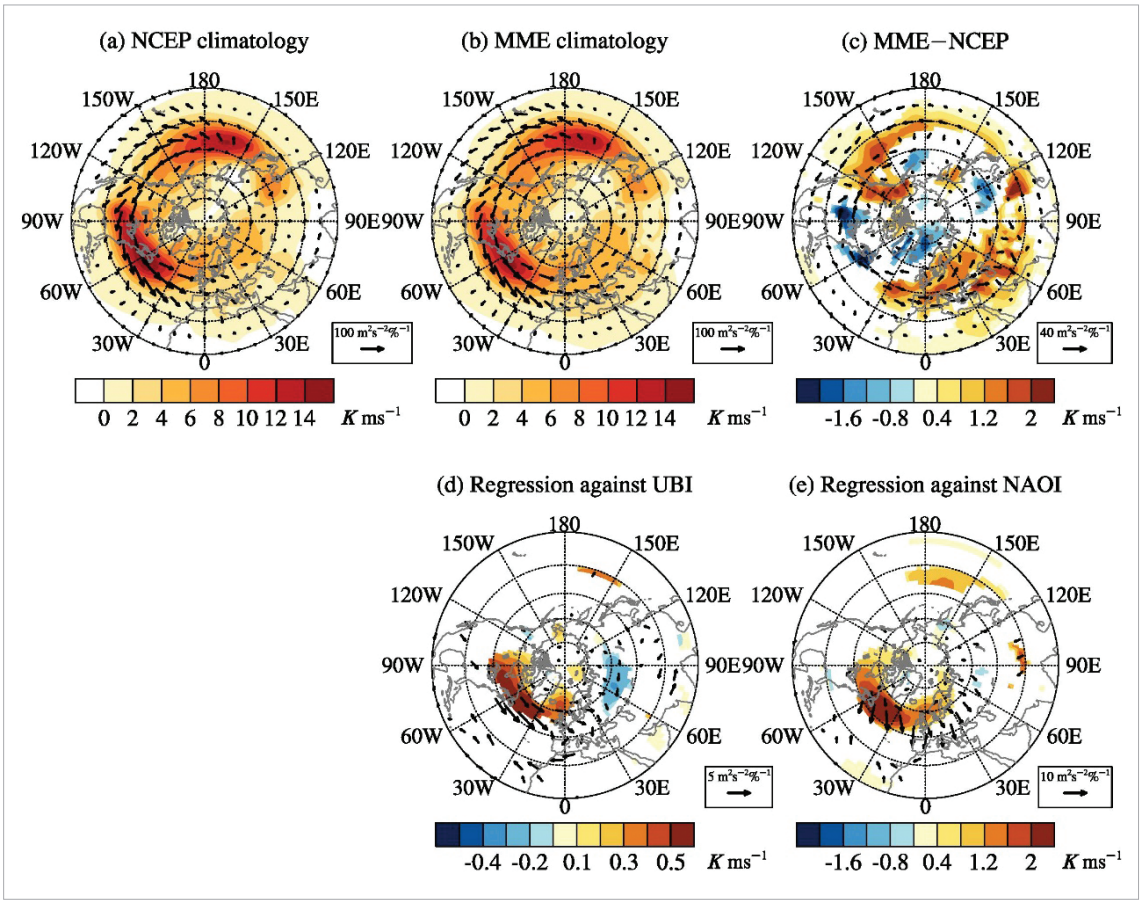

Figure 2. The 55-yr climatology of the high-pass E-vector at the 250-hPa (vector; unit: m^2s^{-2}) and the high-pass poleward heat flux at the 700-hPa (shading; unit: $K\ ms^{-1}$) for (a) the NCEP-NCAR reanalysis datasets and (b) the multiple model ensembles, and (c) their composite difference. (d)–(e). Regression of the E-vector and the heat flux against (d) the UBI (vector; unit: $m^2s^{-2}\ \%^{-1}$; shading; unit: $K\ ms^{-1}\ \%^{-1}$) and (e) the NAOI (vector; unit: m^2s^{-2}; shading; unit: $^K\ ms^{-1}$) across the 25 GCMs. In (c)–(e), vector and shading are significant at the 95% confidence level.

Part II of this study analyzes the Ural blocking (UB)–East Asian winter climate linkage in two representative concentration pathways (RCPs), namely RCP4.5 and RCP8.5, for the period 2006/07 to 2099/2100. Multiple model ensembles (MME) of UBI in 20 CMIP5 GCMs show no apparent increase or decrease in RCP4.5 and 8.5 runs throughout the 21st century. However, a significant increasing or decreasing trend of the Ural blocking index (UBI) is identified in individual GCMs, and the trend appears to be correlated with the trend of the Siberian high index (SHI), which measures the East Asian winter climate (Figure 3). For more details, please refer to Cheung and Zhou (2014a,b).

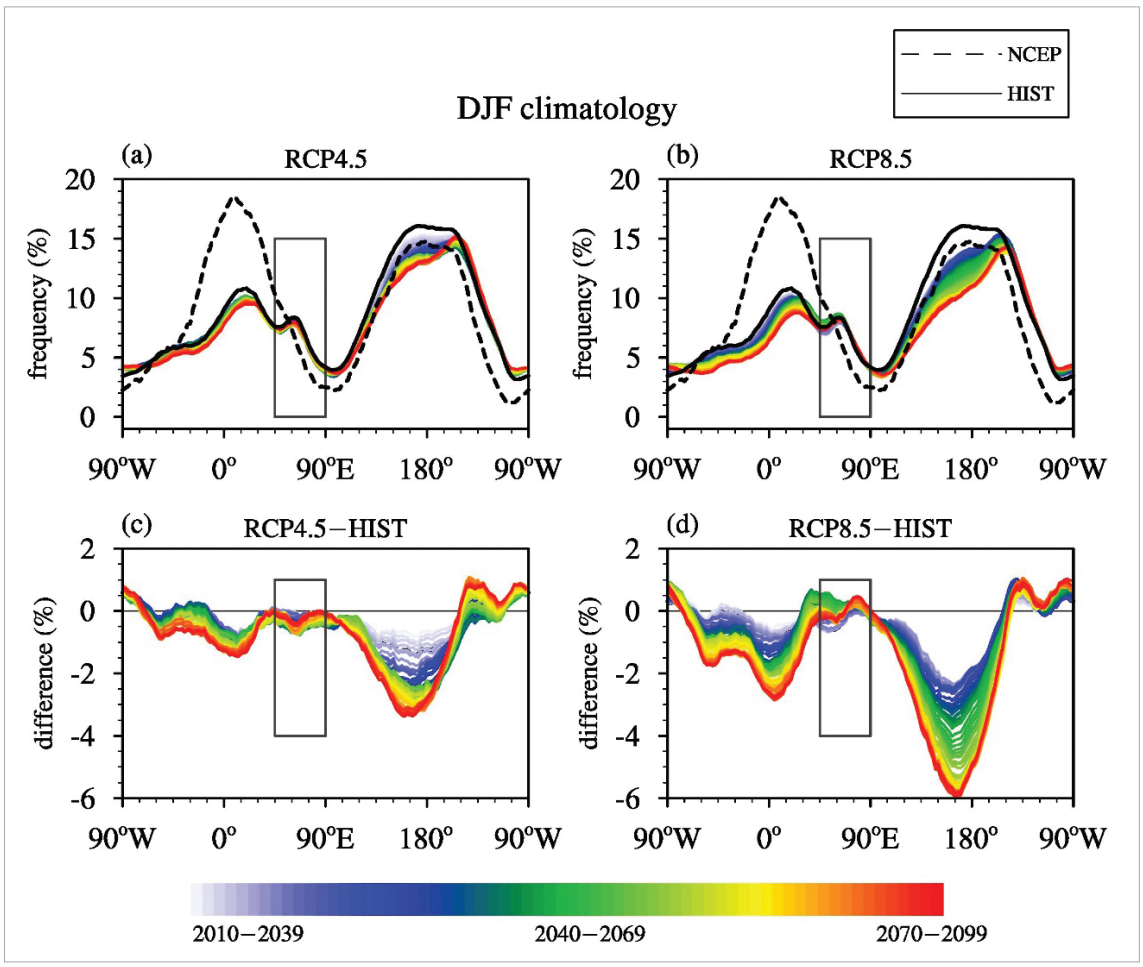

Figure 3. The climatology of winter-mean Northern Hemisphere blocking frequency. (a)–(b) NCEP-NCAR reanalysis datasets, the multiple model ensembles of the historical (HIST) run and 30-year running mean (from 2010–39 to 2070–99) of the RCP4.5 and 8.5 runs. (c)–(d) Difference between the RCP runs and the HIST run. Unit: % of winter days. Note that the square box encloses the Ural sector (45°–90°E).

References:

Cheung H. N. and W. Zhou, 2014a: Implications of Ural Blocking for East Asian Winter Climate in the CMIP5 Models. Part I: Biases in the historical scenario. *Journal of Climate*, doi: 10.1175/JCLI-D-14-00308.1

Cheung H.N. and W. Zhou, 2014b: Implications of Ural Blocking for East Asian Winter Climate in the CMIP5 Models. Part II: Projection and Uncertainty in Future Climate Conditions. *Journal of Climate*, doi: 10.1175/JCLI-D-14-00309.1

B. Climate Variability

B1. Cold Days in Hong Kong and Their Relationship with Large-scale Circulation

(PI: Wen ZHOU)

The increase of the cold days in Hong Kong is related to the recent apparent changes in the large-scale circulation upstream and downstream of the East Asian winter monsoon (EAWM) region: The increase in Ural blocking (UB) enhances cold advection from the polar region and reinforces the Siberian high; and the decrease in a western Pacific (WP)-like index corresponds to increasing meridional gradient of geopotential height over the East Asian Winter Monsoon region (Figure 4). For more details, please refer to Cheung et al. (2014).

During the past decade (2004/05 to 2013/14), the number of cold days in Hong Kong (NCD), as a proxy of the temperature of southern China, appeared to have increased from the historical minimum, in contrast to a remarkable decline in the entire post-war period.

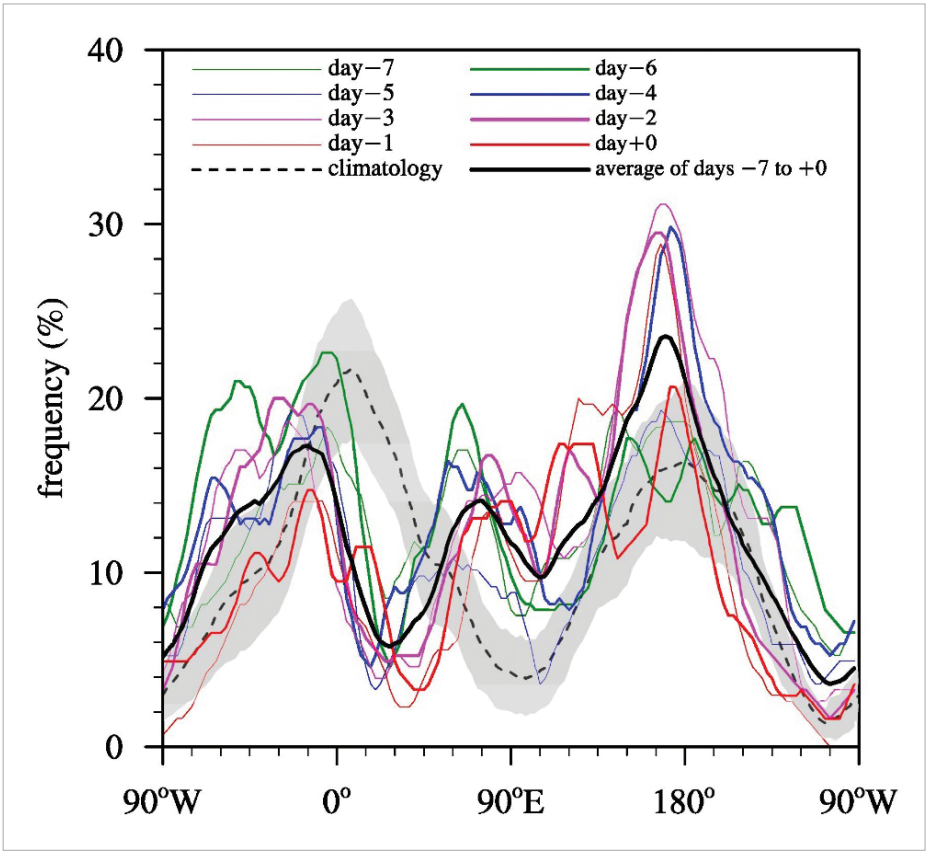

Figure 4. Longitudinal distribution of blocking frequency during the evolution of prolonged cold spells in Hong Kong (colored lines; see legend for description). The gray dashed line and shading indicate the DJF climatology and its half standard deviation, respectively, for the period 1950/51–2009/10. Unit: % of days.

Reference:

Cheung H. N., W. Zhou, S. M. Lee and H W. Tong, 2014: Interannual and Interdecadal Variability of the Number of Cold Days in Hong Kong and Their Relationship with Large-scale Circulation. *Mon. Wea. Rev.*, doi 10.1175/MWR-D-14-00335.1

B2. Multiscale control of summertime persistent heavy precipitation events over South China

(PI: Wen ZHOU)

It is found that the location and strength of the intraseasonal oscillation (ISO) and the synoptic disturbances play a decisive role in controlling the severity and duration of rainfall events over South China. The synchronization and persistence of the enhanced convection and moisture circulation of the ISO and synoptic disturbances jointly contribute to prolonged heavy precipitation over South China, while the weakening and asynchrony of the associated convection and moisture circulation at different timescales result in rainfall events of weaker intensity and shorter duration (Figure 5). For more details, please refer to Li and Zhou (2014).

This study examines persistent and short-lived heavy precipitation events (PHPEs and SHPEs, respectively) in South China during summer in association with large-scale circulation and moisture processes at different timescales.

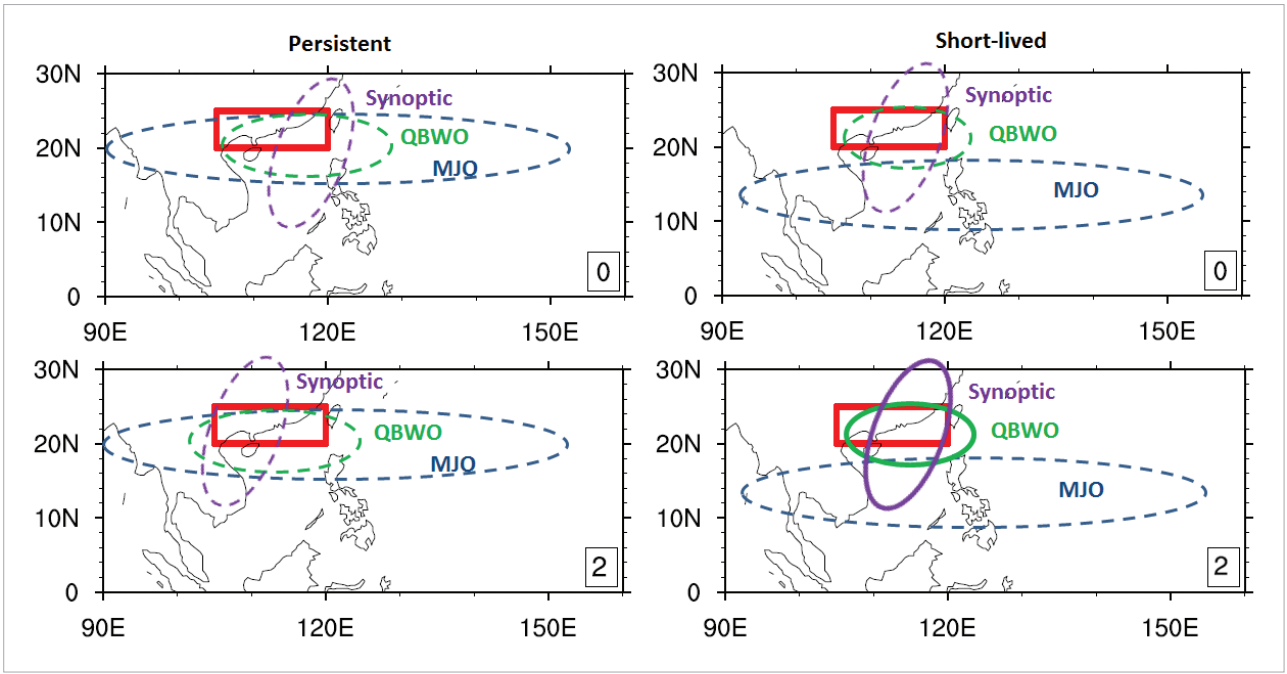

Figure 5. Schematic diagrams illustrating the modulations of the MJO, QBWO, and synoptic disturbances on day 0 and day 2 during persistent (left panel) and short-lived (right panel) heavy precipitation events. Dashed (solid) lines represent enhanced (suppressed) convection and moisture circulations. Thicker (thinner) lines denote convection and moisture circulations with greater (smaller) magnitude.

Reference:

Li. C. Y. and W. Zhou, 2014: Multiscale control of summertime persistent heavy precipitation events over South China in association with synoptic, intraseasonal, and low-frequency background. *Clim. Dyn.*, doi: 10.1007/s00382-014-2347-6.

B3. Assessment of Regional Drought Trend and Risk over China: A Drought Climate Division Perspective

(PI: Wen ZHOU)

The climate division facilitated the evaluation of not only regional but also widespread droughts. Trend evaluation showed that western North China (WNC) has become increasingly wet in recent decades, while northern Northeast China (NNE) has become increasingly dry.

The Yangtze River valley (YZ) tended to experience less and weaker drought after the late 1970s. Southern Northeast China (SNE) and the Southwest China-Tibetan Plateau (SW-TP) showed a decreasing trend in long-term but not short-term SPIs, implying that long-term drought conditions might develop continuously, thus allowing the subsequent droughts to develop more rapidly and with a stronger intensity (Figure 6). For more details, please refer to Li et al. (2015).

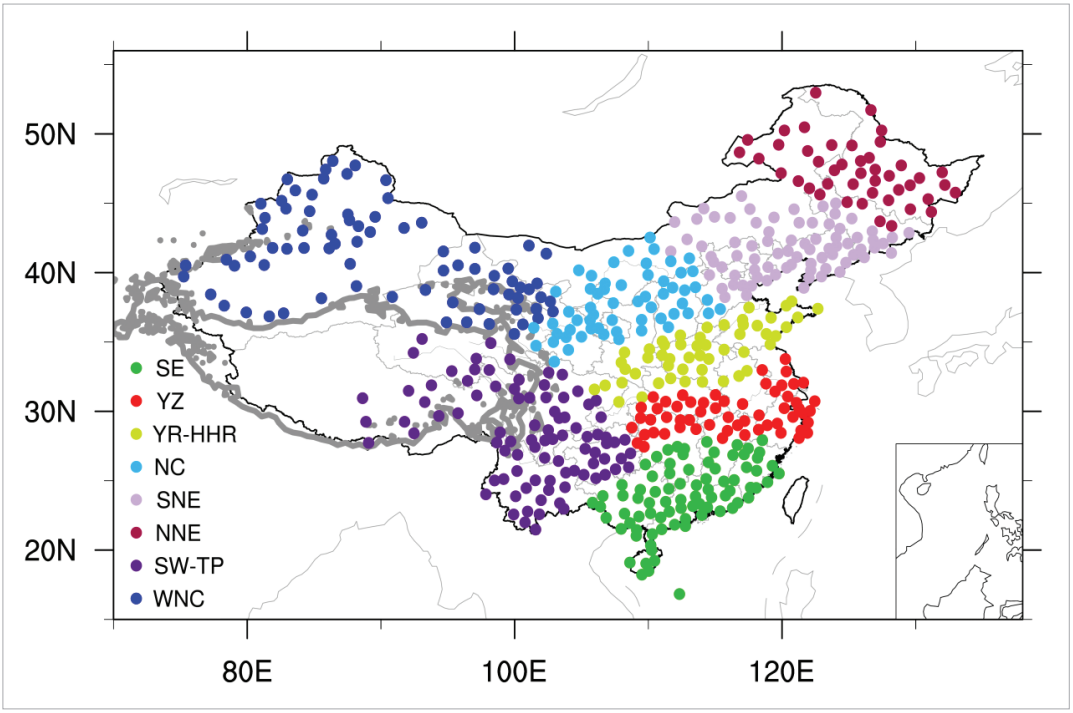

Figure 6. The final scheme of 8 divisions over China. The bold black lines indicate the boundaries of each division and the bold grey line indicates 4000m isohypse, the boundary of the Tibetan Plateau.

Reference:

Li, X. Z., W. Zhou and Y. Q. Chen, 2015: Assessment of regional drought trend and risk over China: A drought climate division perspective. Journal of Climate. (under review)

B4. East Asian Trough in Boreal Winter

(PI: Wen ZHOU)

B4.1 Two typical mobile trough pathways over East Asia in boreal winter

This study investigates the impact on East Asian winter temperature due to two pathways of East Asian mobile trough (EAMT).

The northern and southern paths of EAMT are classified and examined in this study separately. The sum of two paths counts for almost half of total EAMT. On the other hand, the impact on the East Asian winter

temperature are substantially different between them. The stronger temperature fluctuation over Southeast (Northeast) Asia comes with the passage of the southern (northern) EAMT (Figure 7). For more details, please refer to Leung et al (2014).

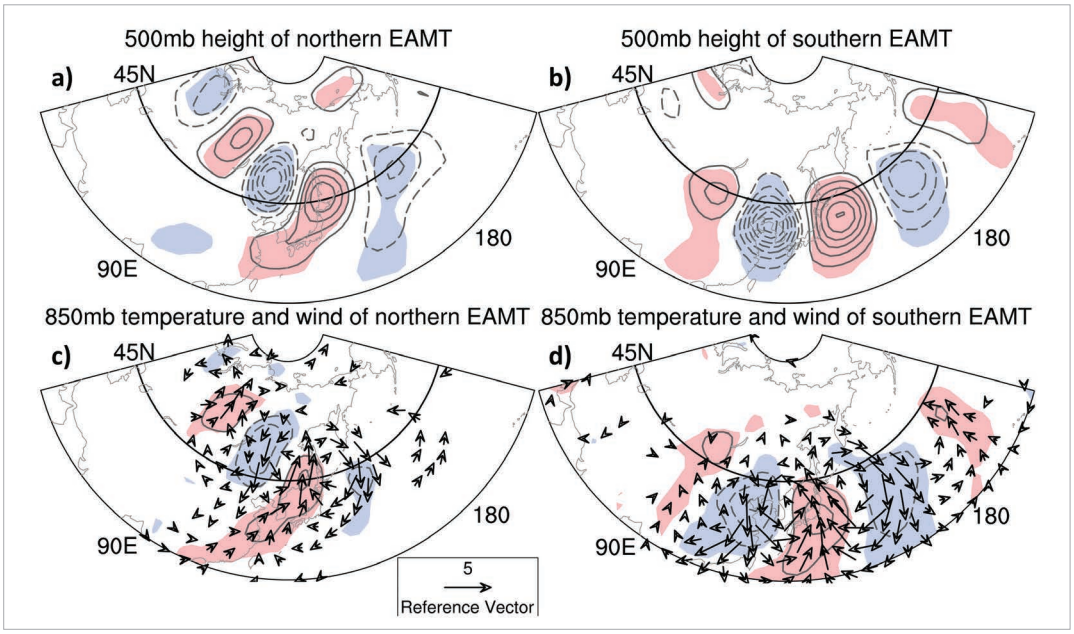

Figure 7. Composite of synoptic 500mb height variations (2-9 days) of a) northern path, and b) southern path of EAMT. c) and d) are similar to a) and b), but for the 850mb temperature (contour) and wind (vector) variations. Red (Blue) shading indicates the 95% significance level for positive (negative) value. Positive (negative) value is shown as solid (dash) contour line.

Reference:

Leung Y. T., H. N. Cheung and W. Zhou, 2014: Energetics and Dynamics Associated with Two Typical Mobile Trough Pathways over East Asia in Boreal Winter. *Climate Dynamics*, doi: 10.1007/s00382-014-2355-6

B4.2 Vertical Structure, Physical Properties, and Energy Exchange of the East Asian Trough

For strong EAT years, the negative longitudinal mean temperature anomalies over the midlatitudes are caused by the adiabatic cooling due to the anomalous rising motion. It alters the available potential energy of zonal mean flow in the midlatitudes in conjunction with the change of the longitudinal mean temperature. So more energy is transferred from the available potential energy of zonal mean flow to that of the EAT which enhances the energy gain of the EAT during winter season (Figure 8). For more details, please refer to Leung and Zhou (2014).

This study examines the changes of energy cycle and energy conversion processes associated with the anomalous strong and weak East Asian trough (EAT).

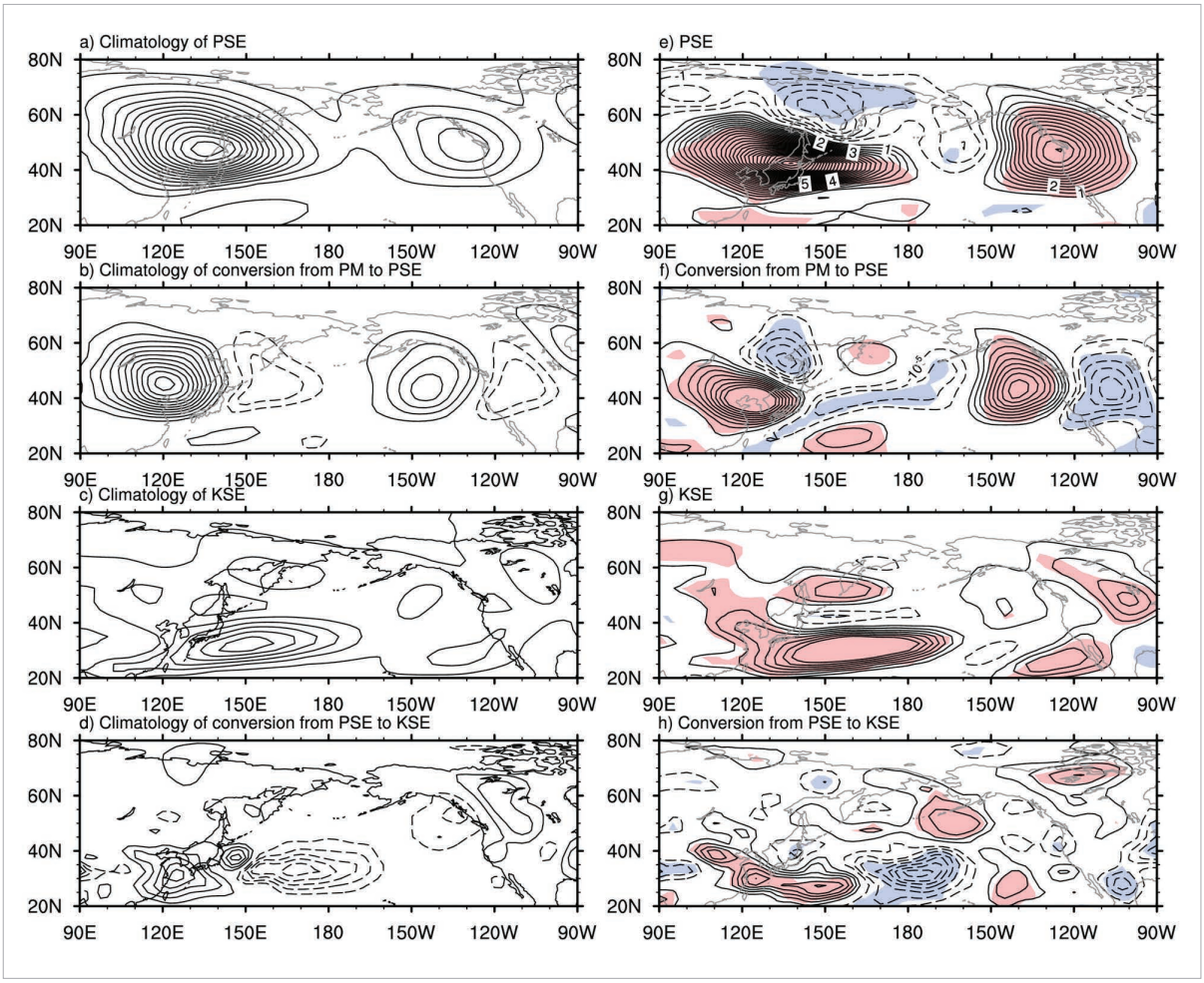

Figure 8. The climatology of a) potential energy of stationary eddy (PSE), b) conversion from available potential energy of zonal mean flow (PM) to PSE, c) kinetic energy of stationary eddy (KSE), and d) conversion from PSE to KSE. e) to h) are similar to a) to d), but for their regressions onto the intensity of the East Asian trough. Red (Blue) shading indicates the 95% significance level for positive (negative) value. Positive (negative) value is shown as solid (dash) contour line.

Reference:

Leung Y. T. and W. Zhou, 2014: Vertical structure, physical properties and energy exchange of the East Asian trough in boreal winter. *Climate Dynamics*, doi:10.1007/s00382-014-2419-7.

B5. Teleconnected influence of tropical Northwest Pacific sea surface temperature on autumn precipitation in South China

(PI: Wen ZHOU)

The interannual variation of autumn precipitation in Southwest China (SWC) and the possible influence of tropical Northwest Pacific (NWP) sea surface temperature (SST) are investigated.

The results of numerical experiments, forced by SST anomalies in the NWP alone, are found to reproduce the observed atmospheric response, indicating that the impact of NWP SST on SWC precipitation is physical and that the moisture conditions over SWC are triggered primarily by the fluctuation of NWP SST. Due to the persistent SST anomaly over NWP from summer to autumn, the NWP SST in the preceding

summer can be considered a predictor for autumn drought in SWC. Furthermore, autumn precipitation in SWC has experienced a significant decrease since 1994, probably maintained by the long-lasting warm NWP SST in recent decades (Figure 9). For more details, please refer to Wang et al. (2014).

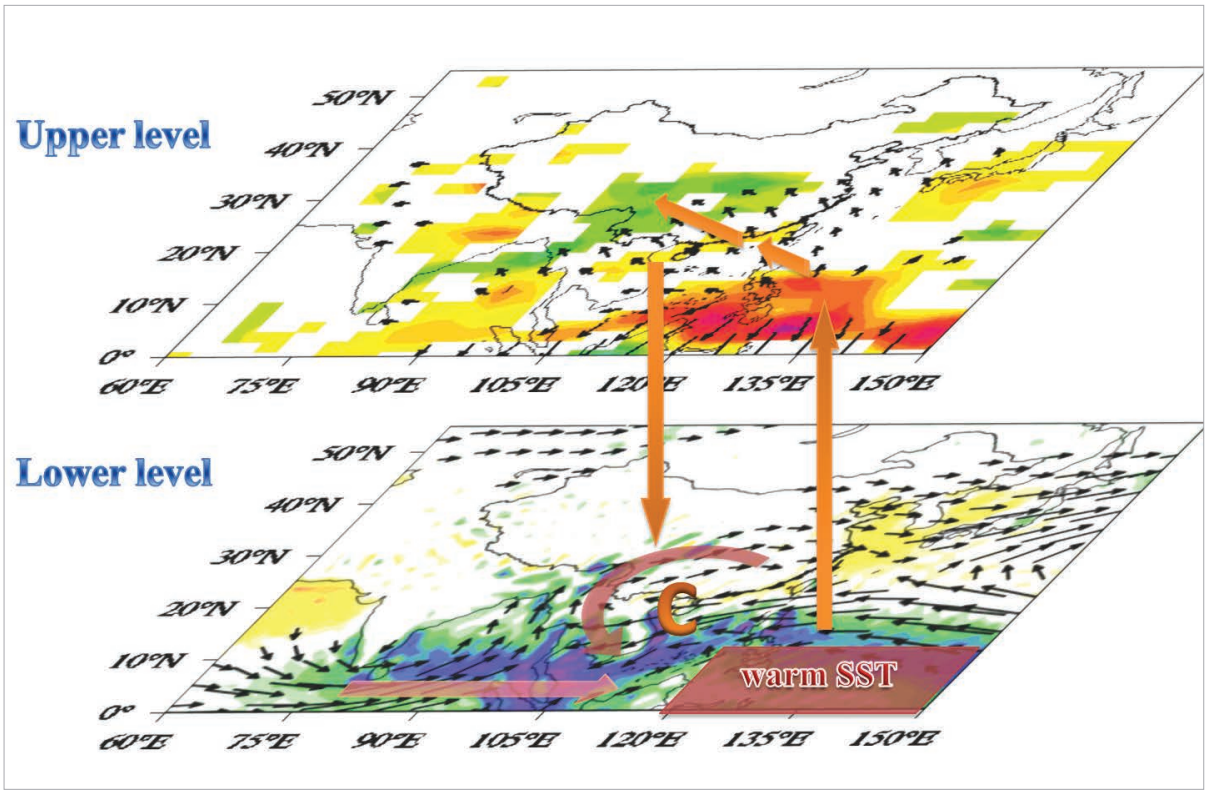

Figure 9. Schematic diagram of the response of atmospheric circulation to NWP SST warming.

Reference:

Wang L., W. Chen, W. Zhou and G. Huang, 2014: Teleconnected influence of tropical Northwest Pacific Sea surface temperature on interannual variability of autumn precipitation in Southwest China. *Climate Dynamics*, doi 10.1007/s00382-015-2490-8.

C. Tropical Cyclone

C1. Variations of Power Dissipation Index in East Asia Region

(PI: Johnny CHAN)

This study examines the variability of power dissipation index (PDI) for different regions in the East Asia region during the period 1960-2013. The annual PDI for a region is calculated as the sum of the PDI, defined as the cube of the maximum sustained wind speed at landfall, of each TC making landfall at that region. Trends in annual PDI are identified in some regions (Korean Peninsula, Zhejiang province, Taiwan and Guangdong province) while interdecadal variations of annual PDI exist in Japan, the Korean Peninsula, Zhejiang province, Guangdong province and Vietnam, with distinct high-PDI and low-PDI

This study identifies the possible trends and interdecadal variations of power dissipation index in different regions of East Asia and a 3-cell model representing the changes in steering flow near the East Asian coast is proposed.

periods. The shift in TC landfall location along the coast of East Asia can be clearly seen from the "time-region" cross section of the 9-year-Gaussian-filtered standardized PDI for the regions (from south to north) Vietnam, Guangdong province, Taiwan, Zhejiang province, the Korean Peninsula and Japan (Figure 10). Before the mid-1970s, the annual PDI are generally higher than normal in the southern regions (Vietnam, Guangdong province and Taiwan) but lower than normal in the northern regions (Zhejiang province and Korean Peninsula). From the mid-1970s to mid-1980s, the annual PDI are below normal in most of the regions, probably due to the lower overall WNP TC activity. In the mid-1980s, an obvious shift to higher-than-normal PDI is observed in Zhejiang province and the Korean Peninsula. The annual PDI for Guangdong province and Japan then become above normal in the early 1990s. After the late 1990s, significant decreases in annual PDI are found in Vietnam and Guangdong province while the annual PDI in the northern regions continue to be higher, resulting in a distribution with higher PDI in the northern regions and lower PDI in the southern regions, which is opposite to that before the mid-1970s. Thus, this change of PDI distribution represents a northward shift in annual PDI along the coast of East Asia during the period 1960-2013.

A singular value decomposition (SVD) analysis of 850-300-hPa winds suggests three major modes which may represent the changes in steering flow near the East Asian coast, affecting the TC tracks and hence the TC landfalls in various regions. The second SVD mode is featured with an anomalous circulation east of Taiwan (Figure 11a) and is related to the changes of annual PDI in Taiwan, Zhejiang, Fujian and Guangdong province. The third SVD mode represents an anomalous circulation east of Japan (Figure 11b) and has an influence on the annual PDI in Japan and the Korean Peninsula. The fourth SVD mode represents an anomalous circulation over the South China Sea (Figure 11c) and has a close relation with the annual PDI in Guangdong province and Vietnam.

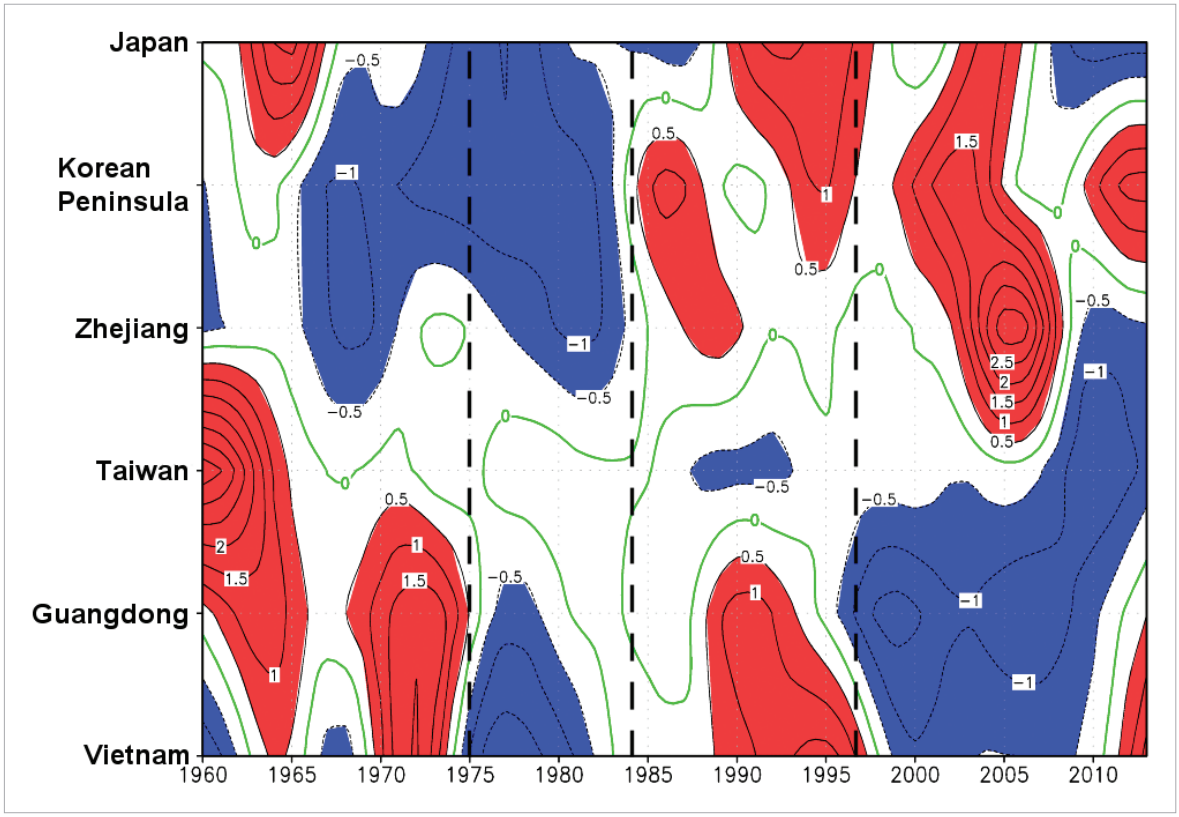

Figure 10. "Time-region" cross section of the standardized PDI for the regions (from south to north) Vietnam, Guangdong province, Taiwan, Zhejiang province, Korean Peninsula and Japan. Red (blue) shadings indicate the PDI > 0.5σ (< -0.5σ). Vertical dashed lines represent the times of occurrence of the significant changes in PDI distribution.

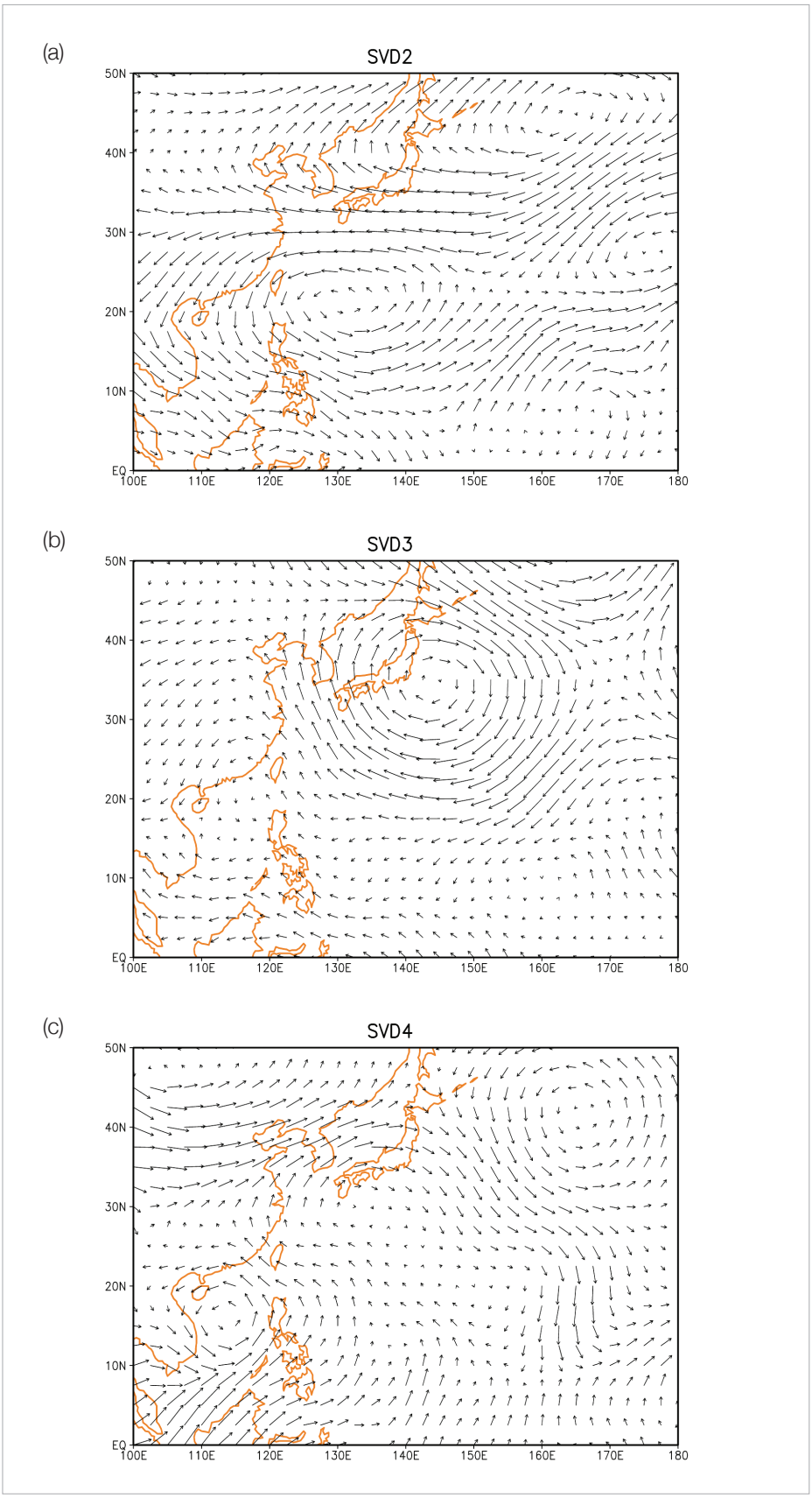

Figure 11. Homogenous correlation maps of 850-300-hPa winds for the (a) second, (b) third and (c) fourth SVD modes and the explained total squared covariance are 13.8%, 8.7% and 7.3% respectively.

C2. *Interdecadal changes in summertime tropical cyclone precipitation over Southeast China*

(PI: Wen ZHOU)

This study examines the changes in tropical cyclone (TC) precipitation and the associated contributing factors over Southeast China during 1960–2009.

Climatologically, tropical cyclone (TC) rainfall accounts for approximately 20–40% of the total rainfall over Southeast China during the boreal summer, and the contribution can even reach 50% for some of the coastal provinces. The dominant mode of TC rainfall reveals a dipole pattern over southern and eastern Southeast China (SSC and ESC), and the associated principal component time series exhibits remarkable interdecadal variations, with two potential change points being identified in the late 1970s and early 1990s (Figure 12). For more details, please refer to Li and Zhou (2014).

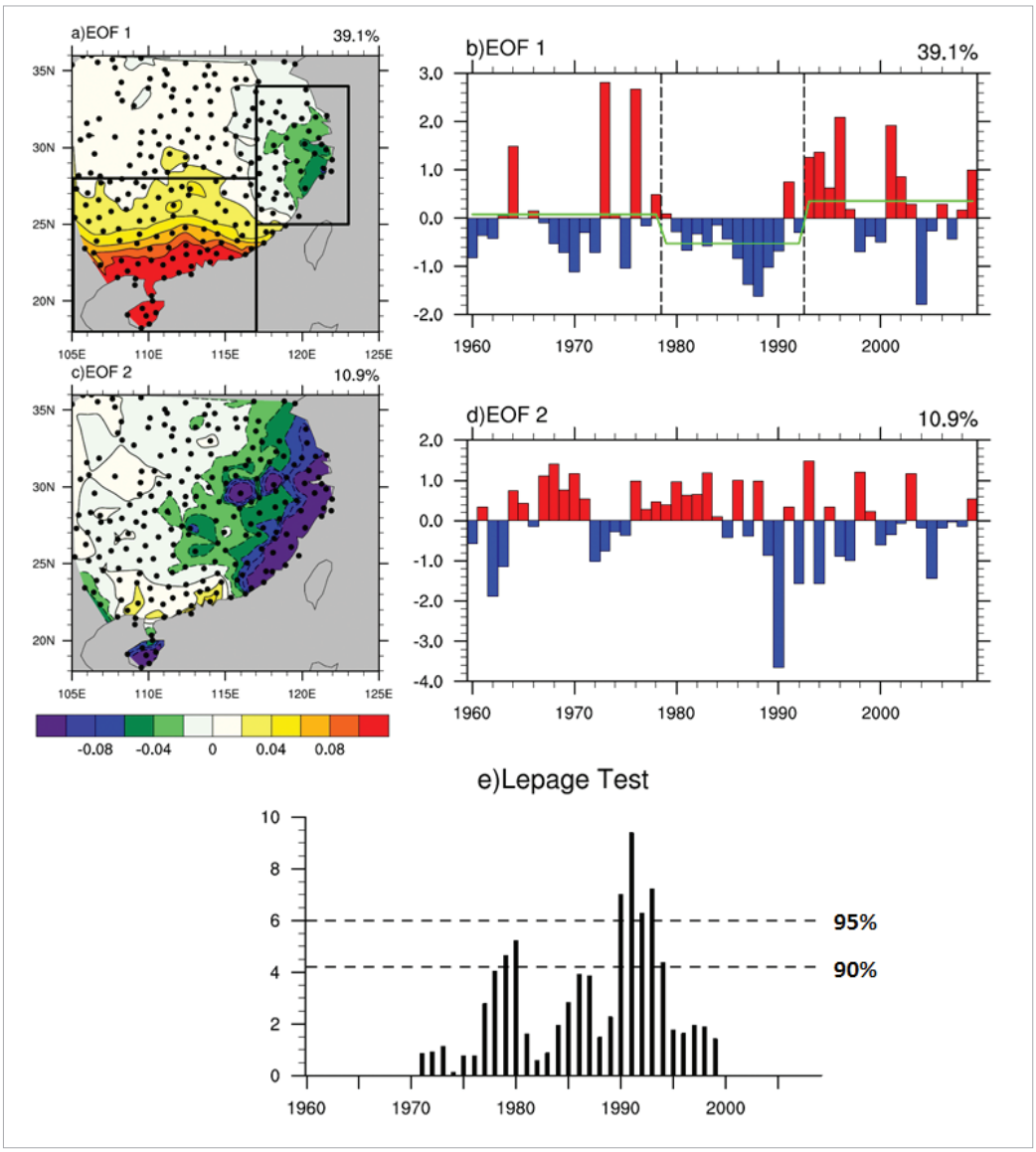

Figure 12. (a), (c) The first two leading EOF modes of TC precipitation, (b), (d) the associated standardized PC time series (bars), and (e) the Lepage test statistics of PC1 during boreal summer 1960–2009. Black dots in (a) represent the stations in Southeast China and the two boxes represent the southern and eastern regions, respectively. The green

line in (b) represents the respective average over the periods 1960–1978, 1979–1992, and 1993–2009. The dashed lines in (e) denote when the Lepage test exceeds 90% and 95% confidence. A year that exceeds the confidence level indicates that the 10-year average of PC1 prior to that year is statistically different from the average following that year.

Reference:

Li. C. Y. and W. Zhou, 2014: Interdecadal changes in summertime tropical cyclone precipitation over Southeast China during 1960-2009. *Journal of Climate*, doi: 10.1175/JCLI-D-14-00246.1

C3. Tropical cyclone-induced rainfall in Hong Kong

(PI: Wen ZHOU)

This study examines the climatological features of tropical cyclone (TC) rainfall in Hong Kong in association with different TC-related parameters, and investigates the changes in TC rainfall, non-TC rainfall, and total rainfall during the past few decades in Hong Kong.

On average, rainfall induced by TCs can account for about 25% of the total precipitation during summer and fall, and the contribution can be even greater in extreme cases. Evaluations of the observed trends of different rainfall indices suggest that the rainfall variability in Hong Kong is considerably affected by the TC rainfall which has a decreasing trend in frequency and intensity in recent decades (Figure 13). For more details, please refer to Li et al. (2014).

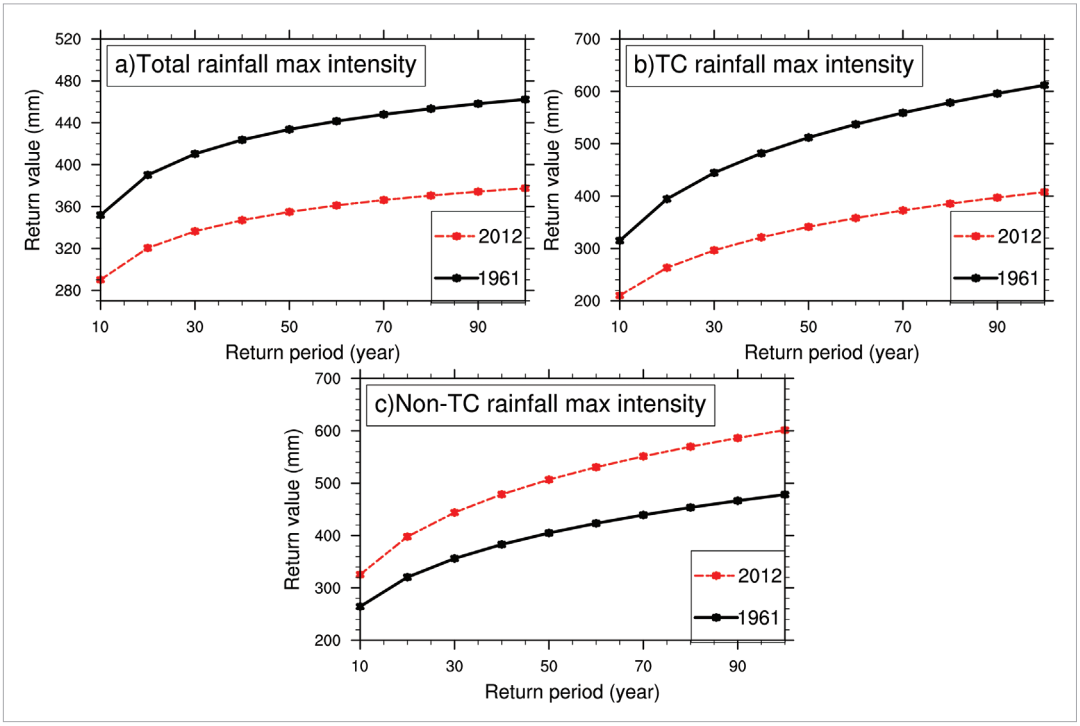

Figure 13. Variations of return values of maximum daily rainfall against return periods in 1961 and 2012 associated with (a) total rainfall, (b) TC rainfall, and (c) non-TC rainfall.

Reference:

Li C. Y., W. Zhou and T C. Lee, 2014: Climatological characteristics, observed trends, and influences of tropical cyclone-induced rainfall in Hong Kong. *Mon. Wea. Rev* doi:10.1175/MWR-D-14-00332.1

D. Air Quality

D1. A novel approach of stable carbon isotope ratio measurement of atmospheric particulate matter (PM) for carbon source identification

(PI: Zhi NING)

A fast and accurate aerosol carbon isotope composition measurement technique has been successfully developed.

A novel approach for measurement of stable carbon isotopic ratio of atmospheric carbonaceous aerosols was developed by hyphenating two instruments namely Sunset Organic Carbon-Elemental Carbon (OC-EC) analyzer and online Carbon Dioxide Stable Isotope Analyzer (LGR, CCIA-36d). The setup diagram is shown in Figure 14. Sensitivity, accuracy and measurement uncertainty of the CCIA were comprehensively investigated by using CO_2 from the standard reference gas of known concentration and isotopic ratio (Figure 15). Offline measurement on different solid samples of varying carbon content was used to assure accurate measurement of CO_2 from detectors of these two instruments. Drift in CCIA measurement due to varying CO2 and water vapor was evaluated and corrected. A Lithium carbonate standard (solid in powder form) from National Institute of Standards and Technology (NIST) was used to validate measurement of $\partial^{13}C$ ratio by CCIA (Figure 16). Keeling approach was applied to separate the ratio in the samples from the mixture of PM sample produced CO_2 and reference gas and a protocol was developed to derive the isotopic composition. This study demonstrates the utility of the tandem operation for isotopic measurement of atmospheric carbonaceous particles. Offline measurement on ambient aerosol and diesel exhaust aerosols produced comparable results of isotopic ratio with their already existing values. Future investigation will develop the method application for online PM carbon isotopic composition measurement.

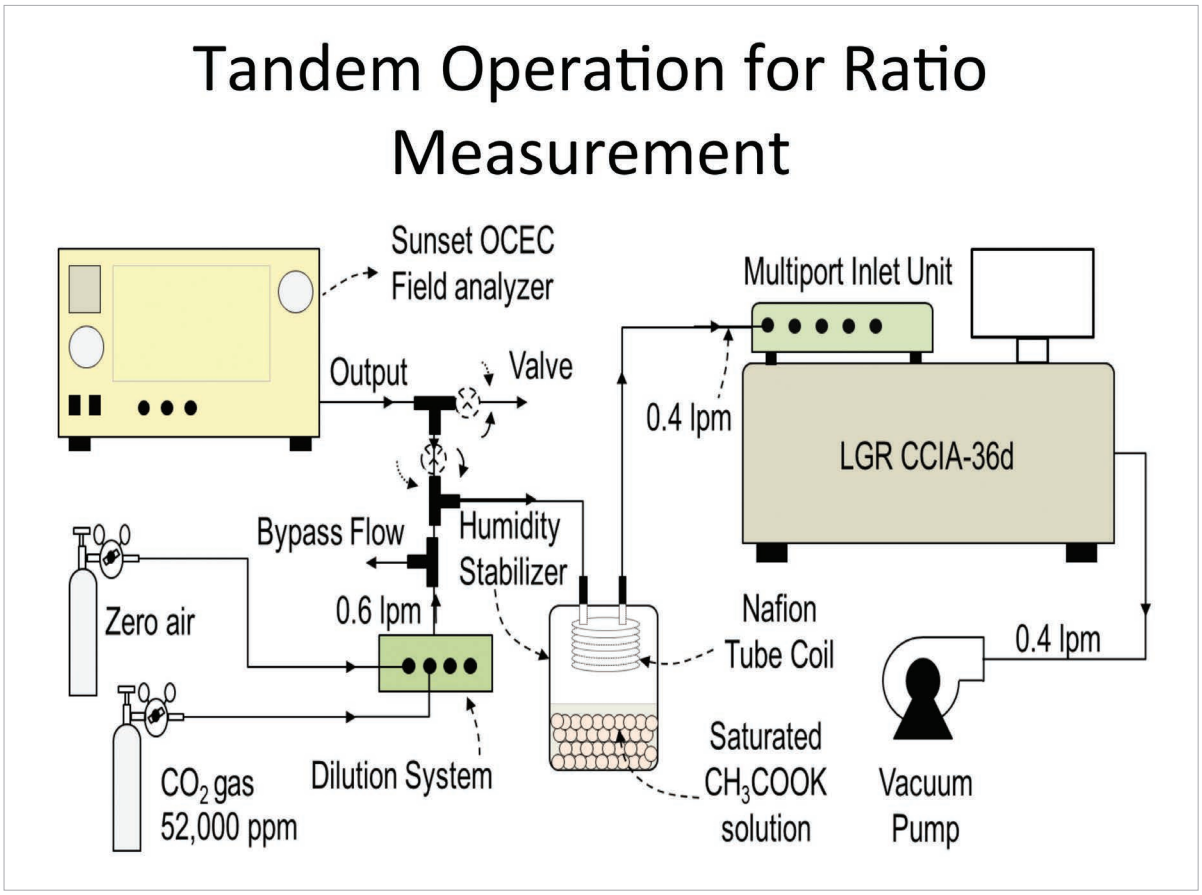

Figure 14. Tandem setup OC-EC analyzer and CCIA

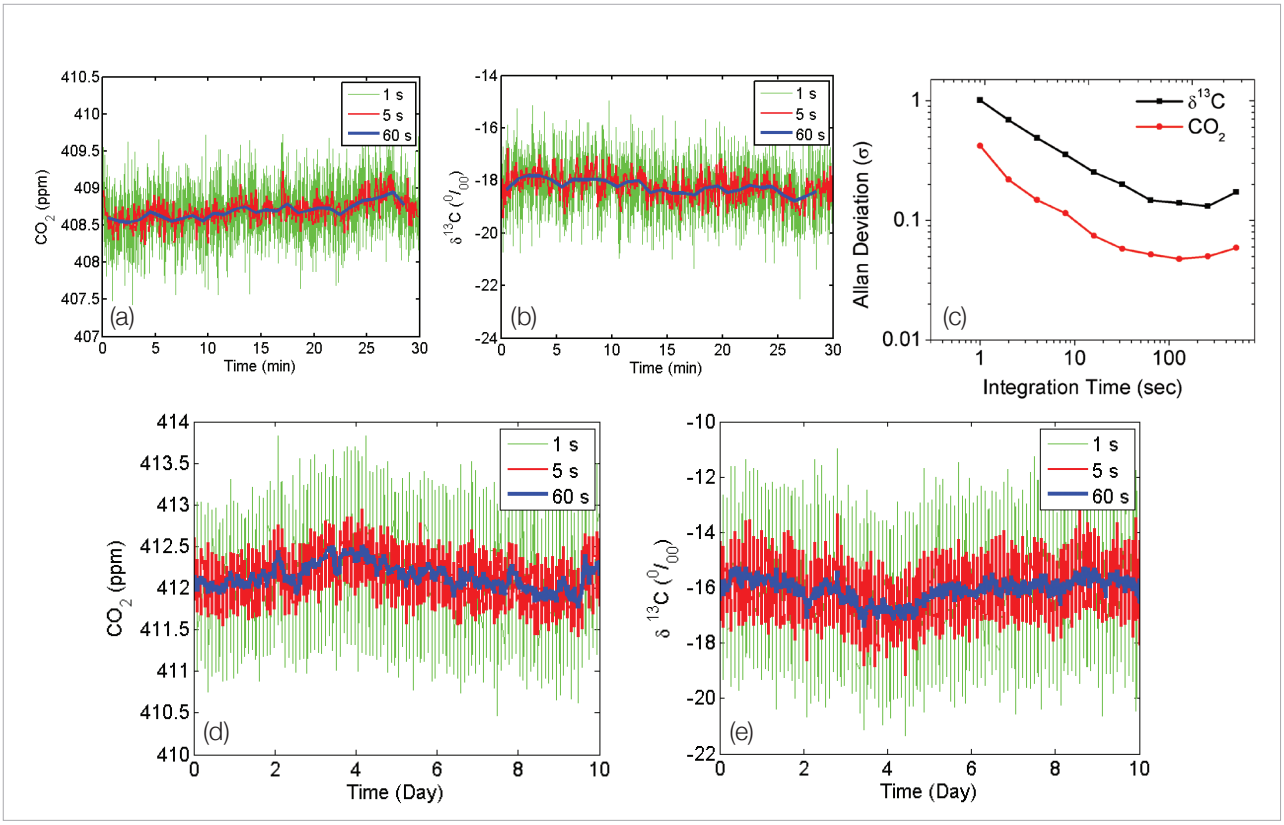

Figure 15. The raw data (1 s), 5 s and 60 s average CO_2 concentration (a), d13C ratio (b) and Allan deviation (c) from a short duration measurement. The raw data (1 s), 5 s and 60 s average CO2 concentration (d) and d13C ratio (e) from a long duration measurement

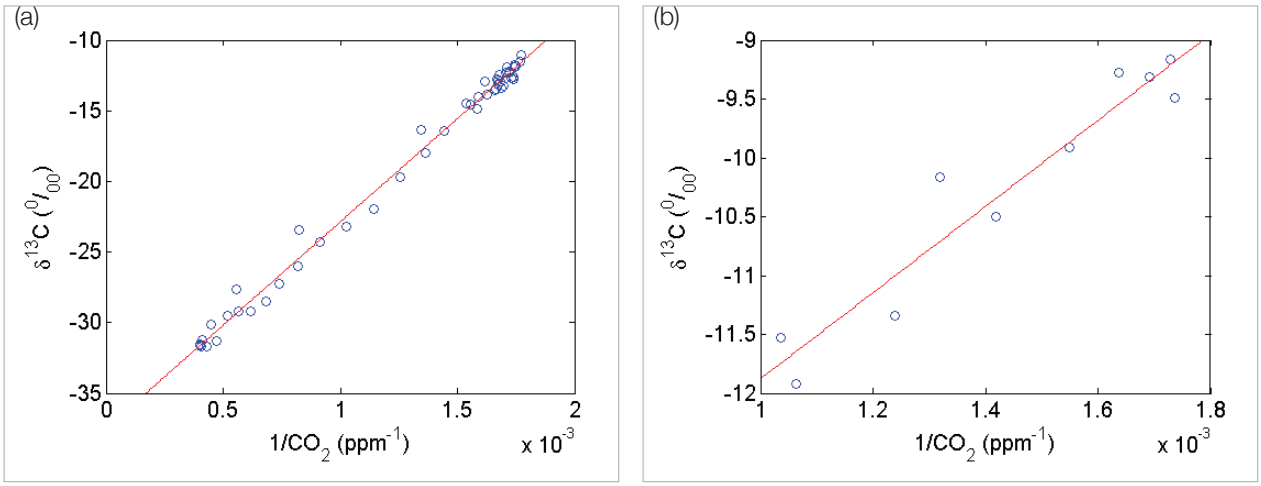

Figure 16. Keeling plot for NIST standard (a) and Diesel exhaust aerosol (b)

Reference:

A novel approach of stable carbon isotope ratio measurement of atmospheric particulate matter (PM) for carbon source identification. 2015 D. Kaul, Z. Ning, D. Westerdahl, X. Yin, R. A. Cary, Submitted to Atmospheric Measurement Techniques.

D2. Water solubility of metals in coarse PM and PM2.5 in typical urban environment in Hong Kong

(PI: Zhi NING)

The water soluble metals profile of PM in typical urban environmental was developed and their relative abundance of anthropogenic concentration was investigated.

An investigation of abundance and solubility of metals in size-segregated particulate matter (PM) was conducted at a typical urban site during the winter of 2011 in Hong Kong. Fourteen elements including Al, Ca, Cd, Cr, Co, Cu, Fe, Pb, Mg, Mn, Mo, Ni, V and Zn by both strong acid digestion and water extraction were analyzed from collected samples using ICP-OES and ICP-MS. The metals in PM showed distinctly different profiles of their distribution between coarse (2.5 μm < d_p < 10 μm) and PM2.5 (d_p < 2.5μm) indicating. The upper continental crustal enrichment factors (CEFs) of the measured metals for two particle size fractions showed that CEFs for nine of fourteen metals in $PM_{2.5}$ were higher than 10 while Cd, Pb, Zn, Mn and Cu were far above 100; whereas for coarse particles, the CEFs of most elements were lower than 10, except for Cd being higher than 100 (Figure 17). Water and acid extractable fractions of coarse PM and $PM_{2.5}$ were analyzed and compared to investigate the transition metals solubility. The water extractable fraction was found to be present mainly in the fine particles, whereas more of the coarse fraction mass remained as insoluble fraction. The results from this study demonstrated large variation of water solubility of metals in urban aerosols in different size fractions and highlighted solubility as an important metric for considering the relation between metals and adverse health effects in epidemiological and toxicological studies.

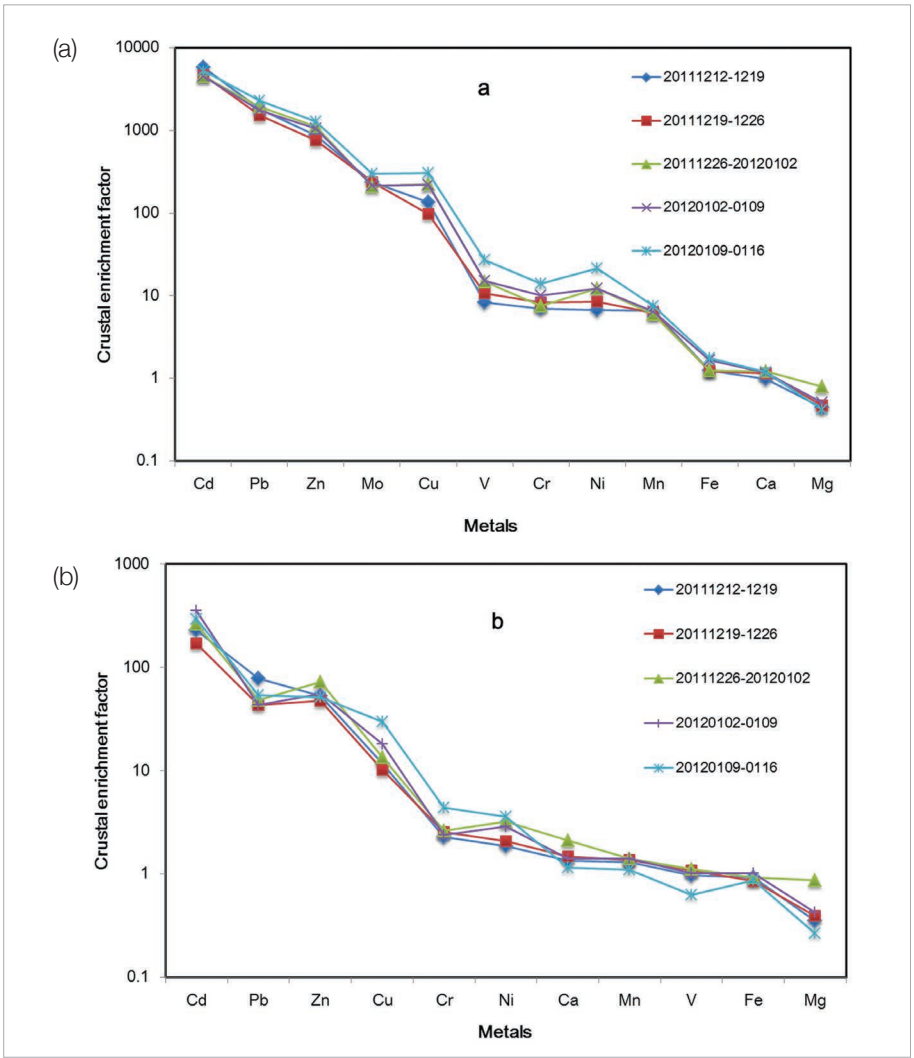

Figure 17. Crustal enrichment factors of elements in (a) $PM_{2.5}$ and (b) coarse particles ranked by abundance.

Reference:

Water solubility of metals in coarse PM and PM 2.5 in typical urban environment in Hong Kong, Sabrina Y.N. Jiang, Fenhuan Yang, Ka Lok Chan, Zhi Ning, *Atmospheric Pollution Research*, 5: 236- 244

D3. Increase of ozone concentrations, its temperature sensitivity and the precursor factor in South China

(PI: Zhi NING)

The long-term trend in ozone concentration in south China has been assessed with discussion on their implication of climate change.

Concerns have been raised about the possible connections between the local and regional photochemical problem and global warming. The current study assesses the trend of ozone in Hong Kong and the Pearl River Delta (PRD) in South China and investigates the interannual changes of sensitivity of ozone to air temperature, as well as the trends in regional precursors. Results reveal, at the three monitoring sites from the mid-1990s to 2010, an increase in the mean ozone concentrations from 1.0 to 1.6 mg m-3 per year (Figure 18). The increase occurred in all seasons, with the highest rate in autumn. This is consistent with trends and temperature anomalies in the region. The increase in the sensitivity of ozone to temperature is clearly evident from the correlation between ozone (OMI Ozone Monitoring Instrument] column amount) and surface air temperature (from the Atmospheric Infrared Sounder) displayed in the correlation maps for the PRD during the prominently high ozone period of July September. It is observed to have increased from 2005 to 2010, the latter being the hottest year on record globally.

To verify this temporal change in sensitivity, the ground-level trends of correlation coefficients/regression slopes are analysed. As expected, results reveal a statistically significant upward trend over a 14-year period (1997-2010). While the correlation revealed in the correlation maps is in agreement with the corresponding OMI ozone maps when juxtaposed, temperature sensitivity of surface ozone also shows an association with ozone concentration, with R=0.5 (Figure 19). These characteristics of ozone sensitivity are believed to have adverse implications for the region. As shown by ground measurements and/or satellite analyses, the decrease in nitrogen oxides (NO_2) and NOx in Hong Kong is not statistically significant while NO_2 of the PRD has only very slightly changed. However, carbon dioxide has remarkably declined in the whole region. While these observations concerning precursors do not seem to adequately support an increasing ozone trend, measured surface levels of formaldehyde, a proxy for volatile organic compound (VOC) emissions, have risen significantly in the PRD (2004 to 2010). Hence, the reactive VOCs in the PRD are likely to be the main culprit for the increase of ozone, as far as precursors are concerned. Despite the prevailing problem, model simulations suggest prospects for improvement in the future.

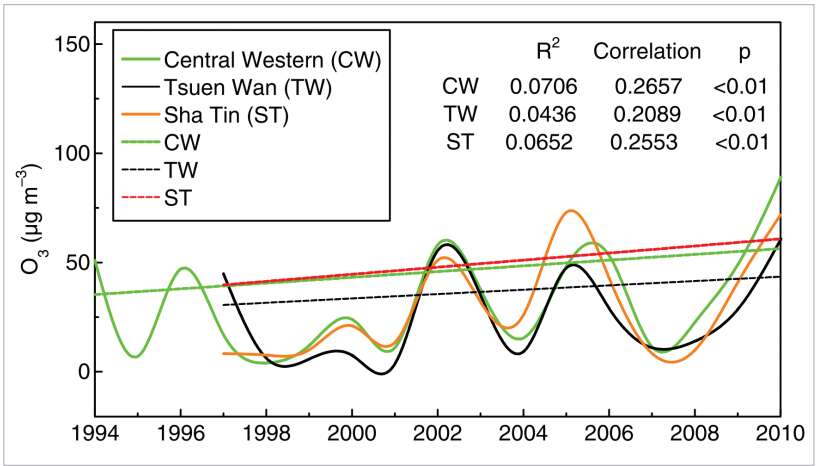

Figure 18. Mean ozone concentrations in Hong Kong (Central Western, Tsuen Wan and Sha Tin)

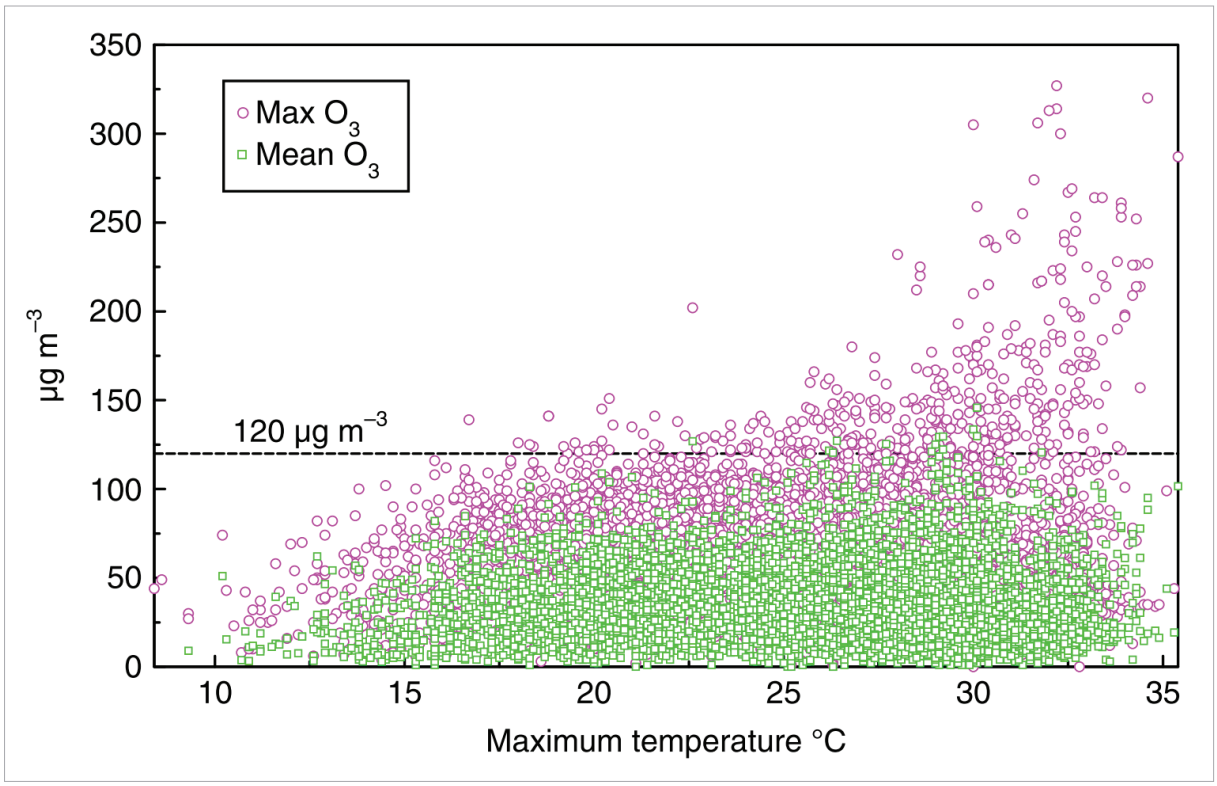

Figure 19. Daily maximum and mean ozone concentrations versus daily maximum temperature in Hong Kong (Central Western)

Reference:

Lee, Y., Shindell, D., Faluvegi, G., Wenig, M., Lam, Y., Ning, Z., Hao, S., & Lai, C. (2014). Increase of ozone concentrations, its temperature sensitivity and the precursor factor in South China. *Tellus B, 66*. doi: http://dx.doi.org/10.3402/tellusb.v66.23455

D4. Observations of tropospheric NO2 by ground based MAX-DOAS and OMI satellite during the Expo 2010 Shanghai

(PI: Nicky LAM)

This study investigates the potential air quality improvement of regional air quality control programs using OMI satellite and MAX-DOAS during the 2010 World Expo in Shanghai.

Four identical Ground based Multi-Axis Differential Optical Absorption Spectroscopy (MAX- DOAS) were used to study the tropospheric nitrogen dioxide (NO_2) from the period of April 2009 to November 2010. A new regularization scheme was applied to the standard inversion algorithm to retrieve tropospheric vertical columns densities (VCDs) of NO_2, where the spatial distribution of NO_2 over Shanghai was studied. The Ozone Monitoring Instrument (OMI) satellite observations as well as meteorological information from National Centers for Environmental Prediction (NCEP) final reanalysis data were used to compare with MAX-DOAS. High correlation between cloud screened MAX-DOAS data and OMI observations were found with the Pearson correlation coefficient (R) ranging from 0.67 to 0.93. Distinct weekday and weekend profiles were observed on some of the stations, which implies that Shanghai has started moving away from heavy industrial activities. The levels of NO_2 reduction from weekday to weekend were as much as 35%. The MAX- DOAS and OMI NO_2 data in 2009 and 2010 were used to represent the prior to and during periods of the Shanghai Expo. The results show that column NO2 in the city center was reduced

up to ~30 %. However, limited reduction was found in the nearby industrial regions. The overall reduction of NO_2 ranged from 7.5% to 14.5% and came from the mobile source controls within the city, rather than the nearby provinces (See Figure 20).

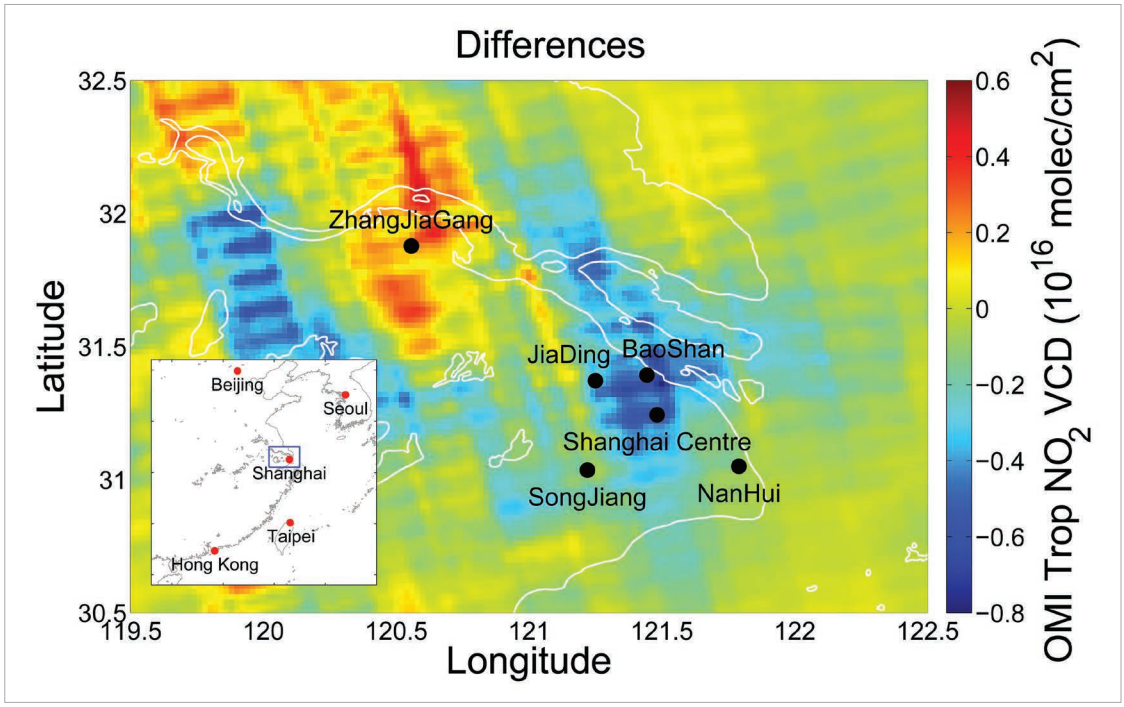

Figure 20. Differences of tropospheric NO_2 VCDs between 2009 and 2010 (2010 – 2009); negative value indicates a reduction of NO_2 levels during the Expo

D5. Developing a hybrid statistical-dynamical approach for predicting air pollution episodes in Hong Kong

(PI: Nicky LAM)

In this study, a system capable of predicting the next-day air quality in Hong Kong was developed using a hybrid statistical-dynamical approach. Generalized additive models (GAMs) were first developed using historical air pollution data with meteorological information (2000 to 2009). By coupling GAMs with the downscaled Global Forecast System (GFS) global products from the Weather Research and Forecasting (WRF) model, daily pollutant concentrations, as well as AQI, were obtained. Our studies found that GFS with WRF (GFS-WRF) performed reasonably well on Respirable Suspended Particulates (RSP), O3 and NO2 concentrations in both urban and sub-urban environments; even with Hong Kong located in the complex terrain region. The Hit Rate (HR) on the categorical forecasts of events with daily air pollution index (API) over 100 ranged from 68-80%. Further investigation of the episodic events due to the presence of tropical cyclones on the effect of the Hit Rate was also evaluated. The model performed much better in the episodic event (HR=95%). Figure 21 shows an example of a tropical cyclone-related episodic event in 29 August 2010. It is clear that the statistical-dynamical model can be a useful tool for air quality prediction for urban and sub-urban sites in Hong Kong.

Air quality forecast predicted by the hybrid statistical-dynamical approach could be a valuable tool for local government to report Air Quality Index (AQI). It is good supplementary information for the high episodic events over the traditional dynamical approach.

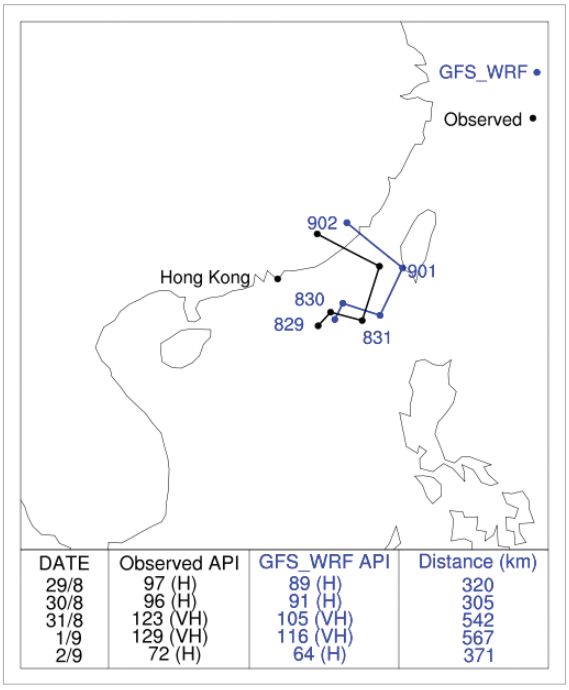

DATE	Observed API	GFS_WRF API	Distance (km)
29/8	97 (H)	89 (H)	320
30/8	96 (H)	91 (H)	305
31/8	123 (VH)	105 (VH)	542
1/9	129 (VH)	116 (VH)	567
2/9	72 (H)	64 (H)	371

Figure 21. GFS-WRF predicted API (blue) with local observation (black) during tropical cyclone Lionrock in the period of 29 August to 2 September 2010. (Figure was adopted from our article submitted to JAWMA)

D6. Evaluation of green infrastructure for near-road pollutant dispersion using micro-scale modelling approach

(PI: Nicky LAM)

In this study, a computational fluid dynamics (CFD) model, ENVI-met, was used to investigate the horizontal and vertical dispersion characteristics of $PM_{2.5}$ under vegetation barrier and green wall. Improvement of air quality was observed 5m to 7m behind the wall in various wind conditions. Reduction of porosity level in the vegetation barrier was found to improve the air quality behind the wall at surface level. Unfortunately, it forces pollutant (i.e., $PM_{2.5}$) to move upward and causes high $PM_{2.5}$ at 5m or above. This increase of concentration could be as much as 150% from its original condition and could greatly affect people who are living in nearby buildings. Similar situations were observed in the green wall where 100% of pollutant was being forced upward, as shown in Figure 22. The removal efficiency of $PM_{2.5}$ is directly proportional to volume of vegetation barrier, where the relative volume of 0.05 – 0.55% resulted in about 0.3 – 0.6% removal and turned out to be insignificant.

This study applied a computational fluid dynamics model, ENVI-met, to investigate the effects of roadside barriers on PM2.5 dispersion characteristics with the effects of changing barrier dimensions.

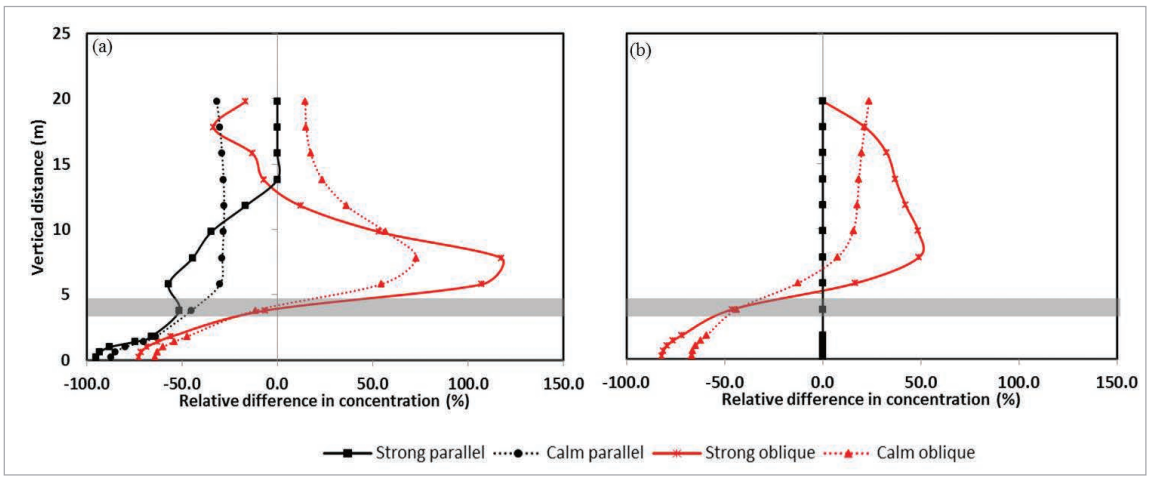

Figure 22. Vertical distribution of average relative difference in concentration at (a) 2m and (b) 10m behind. (Figure was adopted from our article submitted to Journal of Environmental Management)

D7. Hong Kong observatory collaboration on CO2 technology demonstration for WMO reporting

(PI: Zhi NING)

Through successful demonstration of the Febry-Perot Interferometer (FPI) sensor for water interference free water detection in last year, we have been working on expanding the application from laboratory to the field operation. The schematic is shown in Figure 23. Through collaborative effort with the Hong Kong Observatory, we are in preparation to upgrade the FPI sensor with the auto temperature correction algorithm for more challenging ambient measurements. Currently, a weather proof box has been designated in HKO's King's Park monitoring site, and we will deploy our sensor testing platform after preliminary investigation in the laboratory (Figure 24). The collaboration is expected to deliver a comparison of the World Meteorological Organisation designated CO_2 monitor and CityU FPI CO_2 technique.

Collaboration with HKO may promote the next generation greenhouse gas measurement technology to World Meteorological Organisation (WMO) members.

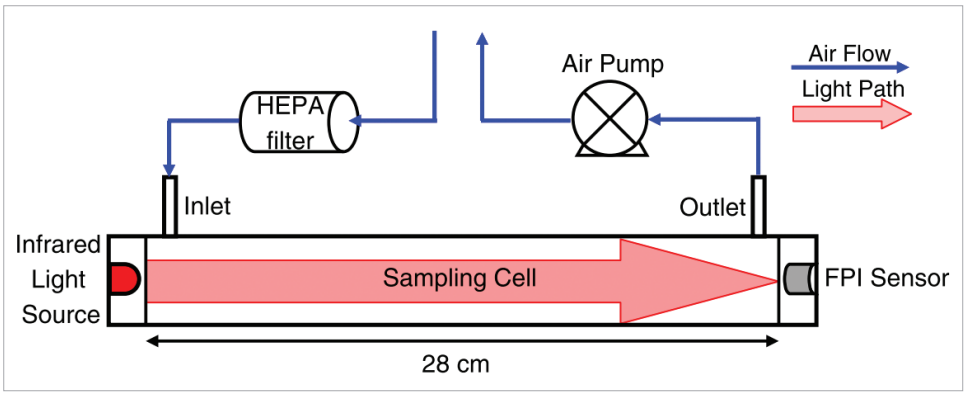

Figure 23. Schematic diagram of the experimental setup of the dispersive infrared spectroscopy measurement

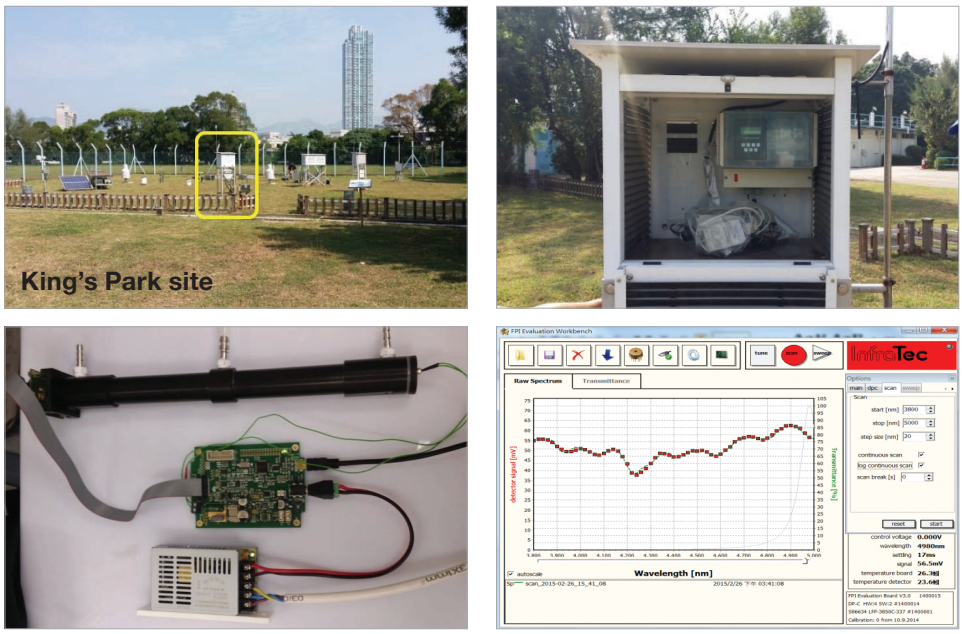

Figure 24. Laboratory tests of new FPI sensor unit

Reference:

K. L. Chan, Z. Ning, D. Westerdahl, K. C. Wong, Y. W. Sun, A. Hartl, M. O. Wenig. Dispersive Infrared Spectroscopy Measurements of Atmospheric CO2 using a Fabry-Perot Interferometer Sensor. *Science of the Total Environment* (IF: 3.258), 472, Pages 27–35. 2013. doi: 10.1016/j.scitotenv.2013.10.105

Publications

Journal Papers

Cheung, H. N. and W. Zhou, 2014: Implications of Ural Blocking for East Asian Winter Climate in CMIP5 GCMs. Part I: Biases in the Historical Scenario. *J. Climate*, **28**, 2203–2216. doi: 10.1175/JCLI-D-14-00308.1

Cheung, H. N. and W. Zhou, 2014: Implications of Ural Blocking for East Asian Winter Climate in CMIP5 GCMs. Part II: Projection and Uncertainty in Future Climate Conditions. *J. Climate*, **28**, 2217–2233., doi: 10.1175/JCLI-D-14-00309.1

Cheung H. N., W. Zhou, S. M. Lee and H W. Tong, 2014: Interannual and Interdecadal Variability of the Number of Cold Days in Hong Kong and Their Relationship with Large-scale Circulation. *Mon. Wea. Rev.*, doi 10.1175/MWR-D-14-00335.1

Choi, Y., K.-S. Yun, K.-J. Ha, K.-Y. Kim, S.-J. Yoon and J. C. L. Chan, 2014: Effects of asymmetric SST distribution on straight-moving Typhoon Ewiniar (2006) and recurving Typhoon Maemi (2003). *Mon. Wea. Rev.*, **141**, 3950-3967.

Huang, W.-R. and J. C. L. Chan, 2014: Dynamical downscaling forecasts of western North Pacific tropical cyclone genesis and landfall. *Clim. Dyn.*, **42**, 2227–2237.

Lee, Y., Shindell, D., Faluvegi, G., Wenig, M., Lam, Y., Ning, Z., Hao, S. and Lai, C., 2014: Increase of ozone concentrations, its temperature sensitivity and the precursor factor in South China. *Tellus B*, **66**, doi:10.3402/tellusb.v66.23455.

Leung, Y. T., Cheung, H. N. and W. Zhou, 2014: Energetics and dynamics associated with two typical mobile trough pathways over East Asia in boreal winter. *Clim. Dyn.*, **44**, 611-1626., doi: 10.1007/s00382-014-2355-6

Leung, Y. T. and W. Zhou, 2014: Variation of circulation and East Asian climate associated with anomalous strength and displacement of the East Asian trough. *Clim. Dyn.*, doi: 10.1007/s00382-015-2504-6.

Leung, Y. T. and W. Zhou, 2014: Vertical structure, physical properties, and energy exchange of the East Asian trough in boreal winter. *Clim. Dyn.*, doi: 10.1007/s00382-014-2419-7.

Li, C. Y. and W. Zhou, 2014: Interdecadal change in South China Sea tropical cyclone frequency in association with zonal sea surface temperature gradient. *J. Climate*. **27**, 5468-5480.

Li, C. Y. and W. Zhou, 2014: Interdecadal changes in Summertime tropical cyclone precipitation over Southeast China during 1960–2009. *J. Climate*, **28**, 1494–1509., doi: 10.1175/JCLI-D-14-00246.1

Li, C. Y. and W. Zhou, 2014: Multiscale control of summertime persistent heavy precipitation events over South China in association with synoptic, intraseasonal, and low frequency background. *Clim. Dyn.*, doi: 10.1007/s00382-014-2347-6.

Li, Y., K. K. W. Cheung and J. C. L. Chan, 2014: Modeling the effects of land-sea contrast on tropical cyclone precipitation under environmental vertical wind shear. *Quart. J. Roy. Meteor. Soc.*, doi:10.1002/qj2359.

Li, Y., K. K. W. Cheung and J. C. L. Chan, 2014: Numerical study on the development of asymmetric convection and vertical wind shear during tropical cyclone landfall. *Quart. J. Roy. Meteor. Soc.*, doi:10.1002/qj2259.

Li, X. Z., W. Zhou, D. L. Chen, C. Y. Li and J. Song, 2014: Water vapor transport and moisture budget over East China: Remote forcing from the two types of El Niño. *J. Climate*. **27**, 8778-8792.

Li, X. Z. and W. Zhou, 2014: Modulation of the Indo-Burma Trough on the Winter Moisture Supply over Southwest China. *Clim. Dyn*, doi: 10.1007/s00382-015-2575-4

Liu, Y. Y., L. Wang, W. Zhou and W. Chen, 2014: Three Eurasian teleconnection patterns: Spatial structures, temporal variability, and associated winter climate anomalies. *Clim. Dyn.*, **42**, 2817-2839.

Qian, C., W. Zhou, Fonh, S. K. and Leong, K. C., 2014: Two approaches for statistical prediction of Non-Gaussian climate extremes: A case study of Macao Hot Extremes during 1912–2012. *J. Climate*, **28**, 623–636., doi: 10.1175/JCLI-D-14-00159.1

Rakowska, A., Wong, K. C., Townsend, T., Chan, K. L., Westerdahl, D., Ng, S., Močnik, G., Drinovec, L. and Ning, Z., 2014: Impact of traffic volume and composition on the air quality and pedestrian exposure in urban street canyon. *Atmospheric Environment*, **98**, 260-270.

Wang, L., W. Chen and W. Zhou, 2014: Assessment of future drought in Southwest China based on CMIP5 multi model projections. *Adv. Atmos. Sci.*, **31**, 1035-1050.

Wang, L., W. Chen, W. Zhou and G. Huang, 2014: Teleconnected influence of tropical Northwest Pacific sea surface temperature on interannual variability of autumn precipitation in Southwest China. *Clim. Dyn.*, doi: 10.1007/s00382-015-2490-8.

Wang W. W., W. Zhou, and D. L. Chen, 2014: Summer High Temperature Extremes in Southeast China: Bonding with the El Niño-Southern Oscillation and East Asian Summer Monsoon Coupled System. *J. Climate*. **27**, 4122-4138.

Wang, W. W., W. Zhou, Y. Li, X. Wang, and D. X. Wang, 2014: Statistical modeling and CMIP5 simulations of hot spell changes in China. *Clim. Dyn.*, doi: 10.1007/s00382-014-2287-1.

Williamson, F., R. Allan, R. D'Arrigo, J. C.L. Chan, R. Gartner, A. D. Switzer and R. J Wasson, 2014: New directions in hydro-climatic histories: Observational data recovery, proxy records and the Atmospheric Circulation Reconstructions over the Earth (ACRE) initiative in Southeast Asia. *Geosci. Lett.*, doi 10.1186/s40562-015-0018-z

Xia J. J., Z. W. Yan, G.S. Jia, H.Q. Zeng, Philip Jones, W. Zhou, A. Z. Zhang, 2014: projections of advanceinthe start of growing season during the 21st century based on CMIP5 simulations. *Adv. Atmos. Sci.*, doi: 10.1007/s00376-014-4125-0.

Ye, K. H., C-Y, Tam, W. Zhou, and S-J. Sohn, 2014: Seasonal Prediction of June rainfall over South China: Model assessment and statistical downscaling. *Adv. Atmos. Sci.*, doi: 10.1007/s00376-014-4047-x.

Staff list

Director

Prof. Johnny CHAN	Dean, School of Energy and Environment Chair Professor of Atmospheric Science

Members

Prof. Ronghui HUANG	Honorary Professor (Academician, Chinese Academy of Sciences)
Prof. Chongyin LI	Honorary Professor (Academician, Chinese Academy of Sciences)
Prof. Peter BRIMBLECOMBE	Associate Dean (Research and Postgraduate Studies) Chair Professor of Atmospheric Environment
Dr. Wen ZHOU	Associate Professor
Dr. Nicky LAM	Assistant Professor
Dr. Keith NGAN	Assistant Professor
Dr. Zhi NING	Assistant Professor

Advisory Committee

Prof. Yihui DING	Academician, Chinese Academy of Engineering
Lord Prof. Julian HUNT	Professor, University College London, Fellow of Royal Society

Researchers

Appointed by Centre

Dr. Frederick Dane WESTERDAHL	Visiting Fellow
Dr. Thomas TOWNSEND	Postdoctoral Fellow
Dr. Cheuk Yin LI	Postdoctoral Fellow
Mr. Kin Sik LIU	Senior Research Assistant
Mr. Hung Ming CHEUNG	Research Assistant
Mr. Chak Hang CHOW	Research Assistant
Mr. Song HAO	Research Assistant
Ms. Xiuzhen LI	Research Assistant
Mr. Fenhuan YANG	Research Assistant
Ms. Xinxin ZHANG	Research Assistant

Guy Carpenter Asia-Pacific Climate Impact Centre
City University of Hong Kong
Tat Chee Avenue, Kowloon,
Hong Kong, China.

Tel: (852) 3442 7359
Email: gcacic@cityu.edu.hk
Website: http://www.cityu.edu.hk/gcacic/

MIX
Paper from responsible sources
FSC™ C102099

Printed on FSC™ Certified Paper with SOY INK